DOI: 10.1002/glia.23933

RESEARCH ARTICLE

Check for updates

Serotonin receptor 4 regulates hippocampal astrocyte morphology and function

Franziska E. Müller¹ | Sophie K. Schade¹ | Volodymyr Cherkas¹ | Laura Stopper² | Björn Breithausen³ | Daniel Minge³ | Hristo Varbanov⁴ | Christian Wahl-Schott⁴ | Svitlana Antoniuk^{1,5} | Catia Domingos³ Valérie Compan⁶ | Frank Kirchhoff² | Christian Henneberger^{3,7,8} |

Correspondence

Evgeni Ponimaskin, Cellular Neurophysiology, Hannover Medical School, Hannover, Germany. Email: ponimaskin.evgeni@mh-hannover.de

Funding information

Deutsche Forschungsgemeinschaft, Grant/ Award Numbers: FOR2795, HE6949/1; HE6949/3, PO732, SFB1089 B03, SFB870 B05, SPP1757, ZE994/2

Abstract

Astrocytes are an important component of the multipartite synapse and crucial for proper neuronal network function. Although small GTPases of the Rho family are powerful regulators of cellular morphology, the signaling modules of Rho-mediated pathways in astrocytes remain enigmatic. Here we demonstrated that the serotonin receptor 4 (5-HT₄R) is expressed in hippocampal astrocytes, both in vitro and in vivo. Through fluorescence microscopy, we established that 5-HT₄R activation triggered RhoA activity via Ga13-mediated signaling, which boosted filamentous actin assembly, leading to morphological changes in hippocampal astrocytes. We investigated the effects of these 5-HT₄R-mediated changes in mixed cultures and in acute slices, in which 5-HT₄R was expressed exclusively in astrocytes. In both systems, 5-HT₄R-RhoA signaling changed glutamatergic synaptic transmission: It increased the frequency of miniature excitatory postsynaptic currents (mEPSCs) in mixed cultures and reduced the paired-pulse-ratio (PPR) of field excitatory postsynaptic potentials (fEPSPs) in acute slices. Overall, our present findings demonstrate that astrocytic 5-HT₄R-Gα₁₃-RhoA signaling is a previously unrecognized molecular pathway involved in the functional regulation of excitatory synaptic circuits.

KEYWORDS

5-ht Zeug, actin, astrocytes, neuronal excitability, RhoA, serotonin

[Correction added on 27 November 2020, after first online publication: author affiliations were updated.]

This is an open access article under the terms of the Creative Commons Attribution License, which permits use, distribution and reproduction in any medium, provided the original work is properly cited.

© 2020 The Authors. GLIA published by Wiley Periodicals LLC

| wileyonlinelibrary.com/journal/glia

¹Cellular Neurophysiology, Hannover Medical School, Hannover, Germany

²Department of Molecular Physiology, Center for Integrative Physiology and Molecular Medicine (CIPMM), University of Saarland, Homburg, Germany

³Institute of Cellular Neurosciences, Medical School, University of Bonn, Bonn, Germany

⁴Institute of Neurophysiology, Hannover Medical School, Hannover, Germany

⁵Nencki Institute of Experimental Biology of the Polish Academy of Science, Warsaw, Poland

⁶Department of Sciences, Brain, Anorexia & Addiction, Nîmes University, Nîmes, France

⁷German Center for Neurodegenerative Diseases (DZNE), Bonn, Germany

⁸Institute of Neurology, University College London, London, UK

⁹Institute of Neuroscience, Lobachevsky State University of Nizhny Novgorod, Nizhny Novgorod, Russia

[#] Evgeni Ponimaskin and Andre Zeug are equally contributing corresponding authors.

1 | INTRODUCTION

Astrocytes are an important component of the brain circuitry. They are highly heterogeneous, exhibiting variations in their appearance and functionality across brain regions and even within substructures, such as the hippocampus (Amundson, Goderie, & Kimelberg, 1992; Lin et al., 2017; Wallraff, Odermatt, Willecke, & Steinhäuser, 2004). Astrocytes contribute to a multitude of brain processes by modulating synaptic plasticity and neuronal activity (Alfonso Araque et al., 2014; Rusakov, Bard, Stewart, & Henneberger, 2014; Ullian, Sapperstein, Christopherson, & Barres, 2001), controlling extra-synaptic space (Flores-Méndez, Mendez-Flores, & Ortega, 2016) and neurotransmitter clearance (Rose et al., 2018; Sibille, Pannasch, & Rouach, 2014), regulating cerebral blood flow (Mishra, 2017), ensuring energy supply to neurons, and orchestrating the rhythms of neuronal firing patterns (Camandola, 2018; Lee et al., 2014; Sheikhbahaei et al., 2018; Stobart & Anderson, 2013).

Over a century ago, astrocytes were first classified as fibrous or protoplasmic based on their morphology (Andriezen, 1893). In recent years, novel approaches and technological progress have enabled great advance in our understanding of the complexity of astrocyte morphology and function (Wu, Pan, Zuo, Li, & Hong, 2017; Zhang & Barres, 2010). Astrocytes ensheath a vast number of synapses, through which they actively control synaptic plasticity and transmission (Araque, Parpura, Sanzgiri, & Haydon, 1999; Chung, Allen, & Eroglu, 2015; Halassa, Fellin, Takano, Dong, & Haydon, 2007). Astrocyte morphology is regulated by small GTPases of the Rho family—including Cdc42, Rac1, and RhoA (for review see Zeug et al., 2018). Experimental findings suggest that Rac1 and Cdc42 promote filopodia formation and outgrowth, whereas RhoA activation triggers filopodia retraction (Hall, 1998; Hall, 2005; Mackay & Hall, 1998).

The importance of Rho GTPases in morphogenesis is widely accepted; however, the upstream signaling components of Rhomediated pathways in astrocytes remain enigmatic. We previously demonstrated that serotonin receptor 4 (5-HT₄R) is coupled to the heterotrimeric $G\alpha_{13}$ protein, leading to selective activation of the small GTPase RhoA, and promoting morphological changes in neuroblastoma cells and hippocampal neurons (Kvachnina, 2005; Ponimaskin, Profirovic, Vaiskunaite, Richter, & Voyno-Yasenetskaya,-2002). In addition to $G\alpha_{13}$, 5-HT₄R can activate heterotrimeric $G\alpha_{5}$ proteins to induce cAMP-PKA signaling (Bockaert, Claeysen, Bécamel, Dumuis, & Marin, 2006; Muller & Jacobs, 2009). Moreover, 5-HT₄R signaling can occur independently of G proteins, leading to activation of proto-oncogene tyrosine kinase Src and extracellular signal-regulated kinase (ERK), and subsequent pERK1/2 phosphorylation (Barthet et al., 2007).

Prior reports describe 5-HT $_4$ R expression by cultured astrocytes in vitro (Parga, Rodriguez-Pallares, Muñoz, Guerra, & Labandeira-Garcia, 2007). Moreover, microarray analysis confirms 5-HT $_4$ R mRNA expression in astrocytes in the brain at postnatal day (P) 7 and P17, and in cultured astrocytes at days in vitro (DIV) 12 (Cahoy et al., 2008). A more recent study revealed age-independent 5-HT $_4$ R expression in astrocytes within several regions of the mouse brain

(Boisvert, Erikson, Shokhirev, & Allen, 2018). However, the impact of 5-HT_4R activity on astrocytic morphology and function remains

In the present study, by combining quantitative molecular microscopy, time-lapse Förster resonance energy transfer (FRET) imaging, and biochemical approaches, we demonstrated that 5-HT $_4$ R was expressed in astrocytes of the mouse hippocampus, and that 5-HT $_4$ R-G $_{\alpha_{13}}$ signaling in astrocytes increased RhoA activity leading to accumulation of filamentous actin structures. We also identified the role of 5-HT $_4$ R-G $_{\alpha_{13}}$ -RhoA signaling in the regulation of astrocytic morphology. Moreover, electrophysiological experiments in mixed cultures and in acute slices revealed that astrocytic 5-HT $_4$ R modifies the function of excitatory hippocampal synapses.

2 | MATERIALS AND METHODS

2.1 | Animals

largely unexplored.

For all experiments wild type and 5-HT_4R -ko animals from the strain B6-Htr4^{tm1comp} (Compan et al., 2004) on a C57BL/6J background were used. Animals were housed and cared for in accordance to directive 2010/63/EU. Mice were kept in a 14 hr light and 10 hr dark cycle with lights on starting at 7 a.m. Animals had access to food and water ad libitum and were kept under standard conditions at $22 \pm 2^{\circ}C$ room temperature (RT) with $55 \pm 5\%$ humidity. Stereotactic injections were done under allowance given by the Lower Saxony State Office for Consumer Protection and Food Safety (TVA16/2206). All experiments were conducted according to the relevant guidelines. For cell culture male and female pups were used while in all other experiments only male mice were investigated.

2.2 | Cell culture

Primary astrocyte cell cultures were prepared as previously described by Wu et al. (Wu et al., 2014) with slight modifications. Whole brains were taken from mice between P1-3 and cells from dissociated hippocampi were seeded at a density of 5×10^4 cells per 12 mm glass coverslip for microscopy in 500 µl plating medium (49 ml Minimal Essential Medium, 1 ml B-27, 500 µl 200 mM glutamine, 500 µl 100 mM sodium pyruvate, 5 μ/ml penicillin, 5 mg/ml streptomycin). On DIV3 the entire plating medium was replaced with 1 ml maintenance medium (49 ml Neurobasal-A medium, 1 ml B-27, 500 µl 200 mM glutamine, 5 μ/ml penicillin, 5 mg/ml streptomycin). With exception of the shRNA experiments, 1/2 of the medium was exchanged on DIV11 with maintenance medium prior to infection of the cells. Astrocytes were used for experiments on DIV14-17. Mixed hippocampal cultures were obtained from dissociated hippocampi of neonatal mice at P0-1 using an optimized protocol (Kobe et al., 2012). At DIV7 cells were infected with AAVs. Cell cultures were maintained at 37°C in a humidified incubator in a 5% CO₂ atmosphere until they were used for experiments at DIV12. During microscopy, cells were kept in a balanced salt solution containing 115 mM NaCl, 5.4 mM KCl,

0981136, 2021, 4, Downloaded from https://onlinelibrary.wiley.com/doi/10.1002/glia.23933 by Deusches Zentrum Für Neurodeg, Wiley Online Library on [11/05/2023]. See the Terms and Conditions

. (https://onlinelibrary.wiley.com/terms-and-conditions) on Wiley Online Library for rules of use; OA articles are governed by the applicable Creative Commons License



1 mM MgCl₂, 2 mM CaCl₂, and 20 mM HEPES, adjusted to pH 7.4 and 290 mOsm with glucose.

Immunohistochemistry and immunocytochemistry

Frozen sections for immunohistochemistry were obtained from brains of 2-month-old mice taken after perfusion with 4% paraformaldehyde (PFA, #0335.3, Carl Roth, Karlsruhe, Germany) in phosphate buffered saline (PBS). Brains were post-fixed for 24 hr in PFA, and then conserved for 24 hr in 10% (wt/vol) sucrose in PBS followed by 24 hr in 15% (wt/vol) sucrose, all at 4°C. Brains were frozen in Isopentan and kept at -80° C before preparing 30 μm thin brain slices. For immunohistochemistry, slices were incubated for 1 hr in 5% BSA in PBS to block unspecific binding sites. Following antibodies were used for staining: S100β (mouse, dilution 1:500, #66028, Abcam, Cambridge, UK), 5-HT₄R (rabbit, dilution 1:500, #ASR-036, Alomone Labs, Jerusalem, Israel), donkey anti-mouse Alexa Fluor 488 (dilution 1:400, #715-545-150, Jackson ImmunoResearch, Ely, UK), goat anti-rabbit Alexa Fluor 546 (dilution 1:400, #A-11035, Invitrogen, Carlsbad, CA), donkey anti-mouse DyLight 649 (dilution 1:400, #715-495-151, Jackson ImmunoResearch, Ely, UK), and goat anti-rabbit Cyanine3 (dilution 1:400, #A10520 Invitrogen, Carlsbad, CA). The blocking peptide against 5-HT₄R (ASR036AG0140, Alomone Labs, Jerusalem, Israel) was preincubated for 1 hr using 1 μg peptide per 1 μg antibody, according to the supplier's recommendations. For STED microscopy, secondary antibodies used were goat anti-rabbit STAR RED and goat anti-mouse STAR 580 (dilution 1:400, #S-11-2015Hp and #S-092017Hp, Abberior, Göttingen, Germany). Slides were sealed using Fluoromount G mounting medium (#0100-01 SouthernBiotech, Birmingham) and 1.5H glass covers for microscopy.

Immunocytochemical stainings were performed on astrocyte cultures at DIV15. Cells were fixed with 4% PFA for 10 min and permeabilized with ice cold methanol for 2 min. Blocking solution (5% (wt/vol) BSA, #8076.4, Carl Roth, Karlsruhe, Germany, in PBS) was applied for 2 hr followed by incubation with primary antibodies against S100β, 5-HT₄R, GFAP (chicken, dilution 1:2000, #ab4674, Abcam, Cambridge, UK), plasma membrane Ca2+ ATPase (PMCA, mouse, dilution 1:1000, #ab2825, Abcam, Cambridge, UK), Trans-Golgi-Network (TGN) 38 (mouse, dilution 1:500, #MA3-063, ThermoFisher Scientific, Waltham, MA), Lamp-1(rat, dilution 1:500, sc-19992, Santa Cruz Biotechnology, Dallas, TX), Calreticulin (chicken, dilution 1:500, #PA-902A, Invitrogen, Carlsbad, CA) and secondary antibodies donkey anti-mouse Alexa Fluor 488, goat anti-rabbit Alexa Fluor 546, donkey anti-chicken DyLight 649, donkey anti-rat DyLight 649 (dilution 1:400, #703-495-155 and #712-495-153, Jackson ImmunoResearch, Ely, UK). For labeling of filamentous (F-) and globular (G-) actin, cultured astrocytes were fixed for 10 min with 4% PFA, permeabilized in 100% acetone for 3 min and then incubated with DNase I linked to Alexa Fluor 488 (9 µg/ml, #D12371, ThermoFisher Scientific, Waltham, MA) and Phalloidin-TRITC (2.5 µg/ml, #P1951, Sigma, St. Louis, MO) in blocking solution for 30 min.

2.4 Adeno-associated-viruses

The FRET-based biosensor RaichuEV-RhoA was a gift from Michiyuki Matsuda (Kyoto University, Japan). This biosensor contains a YPettagged RhoA covalently linked to a mTurquoise-tagged GTPasebinding domain of RBD-Rhotekin. Upon activation, conformational changes within the biosensor lead to changes in the FRET efficiency between acceptor (YPet) and donor (mTurquoise). Because the donor/ acceptor stoichiometry is 1:1, activation of RhoA can be simply quantified by calculation of the acceptor/donor emission ratio. This improved version of the RhoA biosensor developed by the group of Michiyuki Matsuda (Yoshizaki et al., 2003) was cloned into an adenoassociated-virus (AAV) vector under the control of the murine GFAP promoter and AAVs were produced using the AAV-DJ system. Primary astrocytes were infected with 1×10^4 viral genomes per well on DIV11 and live cell imaging was performed on DIV14. Low virus load and comparably short expression time was necessary to ensure only little side effects on the morphology of the cells by the functional RhoA protein within the sensor.

For knockdown of $G\alpha_S$ or $G\alpha_{13}$ proteins, AAVs encoding for specific short-hairpin RNAs (shRNAs) as well as the far-red fluorescent protein TurboFP650 under control of mGFAP promoter were created. Target sequences were 5'-CCCCAACCAGACTA ACCGCCTGTTCAA GAGACAGGCGGTTAGTCTGGTTGTTTT-3' for Gα_S and 5'-CCCGTG TTCCTGCAGTATCTTCTTCAAGAGAGAAGATACTGCAGGAACACTT-TT-3' for $G\alpha_{13}$ (Oligoengine, Seattle, WA).

For the in vitro and in vivo rescue of cell-type specific 5-HT_4R expression, the encoding sequence was cloned into an AAV-vector under control of either GFAP or synapsin promoter leading to expression by astrocytes or neurons, respectively. An enhanced green fluorescent protein (eGFP) was attached to enable visualization of infected cells. For control conditions, cells were infected with AAVs encoding for tdTomato under control of GFAP or synapsin promoters.

5-HT₄R stimulation and RhoA activation assay

Astrocytes were stimulated with BIMU8 (final 10 µM in all experiments; 10 mM stock solution dissolved in H₂O, #4374; Tocris, Bristol, UK), a selective agonist of the 5-HT₄R, or H₂O as a control. In the RhoA activation assay, BIMU8 was applied 5 min prior to cell lysis. To allow remodeling of the actin cytoskeleton, cells were incubated with BIMU8 for 30 min prior to fixation, F- and G-actin staining and subsequent imaging. In some experiments, the selective ROCK-inhibitor Y-27632 (5 or 20 mM stock solution dissolved in H₂O, #1254; Tocris, Bristol, UK) was used (50 μ M in cell culture experiments and 20 μ M in hippocampal slices). It was applied 30 min prior to BIMU8 stimulation for F- and G-actin staining, 20 min in acute slices or 1 hr in cultures prior to electrophysiological recordings.

To test for an increase in activated RhoA after 5-HT₄R stimulation, a RhoA G-LISA Activation Assay Kit (#027BK124, Cytoskeleton Inc., Denver, CO) was used according to the manufacturer's protocol.

2.6 | RNA isolation and real-time quantitative PCR

For investigations of mRNA expression levels, total RNA was isolated on DIV15 of cultured astrocytes using an RNeasy Kit (#74104, Qiagen, Hilden, Germany) according to the manufacturer's protocol. RNA was transcribed subsequently to cDNA by reverse-transcriptase PCR with Super-ScriptIII (#18080-051, ThermoFisher Scientific, Waltham, MA) in a standard reaction setup as suggested by the manufacturer. cDNA was diluted 10x and then used for real-time quantitative PCR (RT qPCR) in a StepOnePlus™ Real-Time PCR System (ThermoFisher Scientific, Waltham, MA) with a ready-to-use 2x TagMan universal MasterMix (#4324018, ThermoFisher Scientific, Waltham, MA). TaqMan probes were used for detecting 5-HT₄R (#Mm00434129_m1), RhoA (#Mm01601614_g1), $G\alpha_S$ (#Mm00530548_m1), $G\alpha_{13}$ (#Mm00494667_m1, all ThermoFisher Scientific, Waltham, MA). GAPDH primers and probe were: fw 5'-TGCACCACCACTGCTTAGC-3', rev 5'-GGCATGGACTGTGGTCAT-GAG-3', probe 5'-6-FAM-CCCTGGCCAAGGTCATCCATGACAAC-TAM-3' (Sigma, St. Louis, MO).

2.7 | Western blot

For Western blot analysis, astrocytes were seeded on 18 mm glass cover slips at a density of 1×10^5 cells per well and lysed at DIV14-17 in RIPA Buffer. Equal amounts of protein were loaded on a SDS-PAGE and then transferred to the membrane. Unspecific binding was blocked with 5% milk in TBS-T buffer for 1 hr at RT. First antibodies (5-HT₄R, rabbit, dilution 1:500, #ASR-036, Alomone Labs, Jerusalem, Israel; $G\alpha_{13}$, rabbit, dilution 1:500, #sc-410, Santa Cruz Biotechnology; $G\alpha_s$, goat, dilution 1:500, #ab101736, Abcam, Cambridge, UK; RhoA, rabbit, dilution 1:500, #2117S, Cell Signaling Technology, Danvers, CO; GAPDH, mouse, dilution 1:2000, #MAB374, Merck Millipore, Burlington, VT; all in 5% milk and $G\alpha_{12}$, rabbit, dilution 1:500, #sc-409, Santa Cruz Biotechnology; Gα_α, rabbit, dilution 1:500, #sc-393, Santa Cruz Biotechnology; Gα_i, rabbit, dilution 1:1000, #5290, Cell Signaling Technology, Danvers, CO; all in SignalBoost enhancer solution #407207, Merck Millipore) were incubated at 4°C overnight. Secondary antibodies (goat anti-rabbit HRP and rabbit anti-mouse HRP, #31460 and #31455, ThermoFisher Scientific; donkey anti-goat HRP, #sc-2056, Santa Cruz Biotechnology; all 1:400 in 5% milk) were allowed to bind for 1 hr at RT. Blots were developed using SuperSignal West Femto substrate (#34096, ThermoFisher Scientific).

2.8 | Microscopy

Microscopic investigation was performed using Zeiss LSM780 with a LD C-Apochromat ×40/1.2 W objective and Zen2013 imaging software in online-fingerprinting mode with previously defined spectra for each fluorescent protein and dye obtained from single staining. Live cell imaging of RhoA activity in astrocytes with the FRET-based biosensor RaichuEV-RhoA was

performed at 37° C in a continuous time series. Z-stacks of the same cell were acquired in both channels every 20 s using Zeiss Definite Focus to maintain focus during long-term imaging. Cells were recorded for 10 min with application of 10 μ M BIMU8 or H₂O after 5 min of imaging.

In experiments with F- and G-actin, astrocytes were labeled with a GFAP antibody, while in the shRNA experiments TurboFP650 was expressed under control of the GFAP promoter. Stimulated emission depletion (STED) imaging was conducted on an Abberior STEDYCON with an Olympus UPlanSApo $\times 100/1.40$ oil objective. Excitation wavelengths were 594 and 640 nm for STAR 580 and STAR RED, respectively, while depletion wavelength was 775 nm. Images were acquired with a pixel size of 25 nm (1,232 \times 1,116 pixels, 31 μ m \times 28 μ m) and a pixel dwell time of 20 μ s. A total of 17 z-planes were acquired with 1 μ m distance. Image analysis was done using Matlab (Mathworks).

2.9 | In vitro electrophysiological recordings

Whole-cell patch-clamp recordings of neurons in mixed hippocampal cell cultures prepared from 5-HT₄R-ko animals were acquired in voltage-clamp mode using an EP-C-10 USB amplifier controlled by PatchMaster software (HEKA, Lambrecht, Germany) at RT. The extracellular solution contained (in mM): NaCl 150, KCl 1, CaCl₂ 2, MgCl₂ 1, HEPES 10, glucose 10, glycine 0.01 and was adjusted to pH 7.3 and 320 mOsm. Gabazine (1 μ M) and Tetrodotoxin (TTX, 1 $\mu\text{M})$ were always present in the extracellular solution to block γ-aminobutyric acid type A (GABA_A) receptors and sodium channels, respectively. The intracellular solution contained (in mM): KMeSO₃ 125, KCl 10, Na₂Phosphocreatine 5, EGTA 0.5, MgATP 4, Na₂GTP 0.3, HEPES 10, was adjusted to pH 7.3 and 290 mOsm. Patch electrodes were pulled to reach a resistance of 3-6 M Ω . Postsynaptic currents were low-pass filtered (2.9 kHz) and digitized at 20 kHz. The access resistance was monitored throughout the recordings (5 mV steps every 2 min). Recordings with an access resistance of >50 M Ω or a leak current >200 pA were discarded. Miniature excitatory post synaptic currents (mEPSCs) were detected using Matlab (Mathworks) and reviewed manually to check for detection/analysis errors.

2.10 | Stereotactic injections

About 8–10 weeks old male 5-HT $_4$ R knockout animals were stereotactically injected to the CA1 region of the hippocampus using following coordinates relative to bregma: anterior/posterior –0.19 mm, lateral +/–0.15 mm, ventral –0.16 mm. Animals received 1 μ l of AAV-hGFAP-5-HT $_4$ R-eGFP (1.5 × 10 8 viral particles/ μ l) and AAV-hGFAP-tdTomato (1 × 10 7 vg/ μ l) each separately in both hemispheres in alternating order. Three weeks postinfection, animals were sacrificed and electrophysiological recordings were performed in acute hippocampal brain slices.

2.11 | Electrophysiological recordings in acute slices

Slice experiments were performed as previously described (Minge et al., 2017). Briefly, acute, 300 µm thick slices of the dorsal hippocampus were cut with a ceramic blade on a vibratome (Campden Instruments LTD, Loughborough, England) in an ice-cold slicing solution containing (in mM): NaCl 60, sucrose 105, KCl 2.5, MgCl₂ 7, NaH₂PO₄ 1.25, ascorbic acid 1.3, sodium pyruvate 3, NaHCO₃ 26, CaCl₂ 0.5, and glucose 10 (osmolarity 300-310 mOsm). Slices were then kept in this solution at 34°C for 15 min. Another extracellular solution was used for storage at RT and during experiments in a submerged recording chamber at 34°C containing (in mM): NaCl 126, KCl 2.5, MgSO₄ 1.3, NaH₂PO₄ 1.25, NaHCO₃ 26, CaCl₂ 2, and glucose 10 (osmolarity 297-303 mOsm). All solutions were continuously bubbled with 95% O2/5% CO2. For recordings of extracellular field excitatory postsynaptic potentials (fEPSPs), patch pipettes (3-4 $M\Omega$) were filled with extracellular solution and inserted into the CA1 stratum radiatum near astrocytes expressing 5-HT₄R-eGFP or tdTomato respectively, visualized by 2-photon excitation fluorescence microscopy (Olympus FV10MP, Tokyo, Japan or Scientifica, Uckfield, UK). fEPSPs were evoked by electrical stimulation (100 µs) of CA3-CA1 Schaffer collaterals using a bipolar concentric stimulation electrode (FHC) placed in the stratum radiatum 200-300 µm from the recording site. Basal synaptic transmission (fEPSP slope) was quantified by recording fEPSPs over a range of stimulations intensities (25, 50, 75, 100, 150, 200, and 300 μA). Afterwards, the paired-pulse ratio (PPR; fEPSP slope 2/fEPSP slope 1) of two consecutively evoked fEPSPs was measured. In these experiments, the stimulation intensity was adjusted to elicit fEPSPs with half-maximal slope. The stimulus intensities did not differ between experimental groups in control conditions (5-HT₄R knockout: $85.86 \pm 7.92 \,\mu\text{A}$, n = 14; rescue: $83.18 \pm 5.92 \,\mu\text{A}$, n = 11, p = .799, unpaired two-tailed Student's ttest) or in the presence of 20 µM Y27632 (5-HT₄R knockout: 99.0 \pm 9.67 μ A, n = 12; rescue: 97.85 \pm 6.62 μ A, n = 13, p = .784, Mann-Whitney U-Test). The inter-stimulus intervals 25, 50, 100, 200, and 400 ms were used. fEPSPs were recorded using MultiClamp 700B amplifiers (Axon Instruments, Molecular Devices, San Jose, CA) in current clamp mode and digitized at 20 kHz (Bessel filter set to 4 kHz). Offline analysis of fEPSP slopes was performed using Clampfit (Molecular Devices).

2.12 | Image analysis

Microscopic data of F- and G-actin were analyzed using Matlab. Steps in the evaluation process of each channel included background correction, scaling to the 99.9% percentile of intensity of the control condition of each experiment and thresholding using the unimodal background-symmetry method. A z-maximum projection was calculated from averaged actin intensity ($I = \sqrt{I_{F-actin}^2 + I_{G-actin}^2}$). Both the voxel based ratio between F- and G-actin ($R = \frac{I_{F-actin}}{I_{G-actin}}$) as well as the F-actin fraction ($F_{F-actin} = \frac{I_{F-actin}}{I_{F-actin}^2 + I_{G-actin}^2}$) were calculated for visualization

and statistical analysis. Statistical analysis was done with Prism software (Graph Pad Software, San Diego, CA).

2.13 | Statistical analysis

Statistical analysis was done using GraphPad Prism7 software. Two-tailed t-test (paired or unpaired) was applied to determine the statistical difference between two experimental groups. Analysis of variance (ANOVA, one-way or two-way where appropriate) followed by a post hoc test was used for multiple comparisons. A *p*-value <.05 was considered statistically significant within each test. The exact *p*-values are presented in the graphs or stated in the figure legends with respective details. Data presented as bar graphs represent mean values ± SEM. Box plots show median and interquartile range with whiskers from minimum to maximum values. Quantitative analysis of western blots was done by the sum of replicates method.

3 | RESULTS

3.1 | Hippocampal astrocytes express 5-HT₄R in vivo

To understand the functional role of 5-HT₄R in astrocytes, we first investigated whether this receptor was expressed on hippocampal astrocytes. Immunohistochemical staining revealed 5-HT₄R localization on cells positive for the astrocytic marker S100ß within the hippocampal formation of the adult mouse brain (Figure 1a-c). We confirmed antibody specificity using a corresponding blocking peptide, and by staining of hippocampal slices prepared from 5-HT₄R-ko mice (Figure S1a-c). Since it appeared not all astrocytes were expressing 5-HT₄R, we quantified the percentage of astrocytes positive for the 5-HT₄R in the hippocampus and in the other brain regions. We found that $33 \pm 12\%$ of astrocytes in the hippocampus express the 5-HT₄R, while in other brain regions percentage of 5-HT₄R positive astrocytes was lower (cortex 9 ± 3%, midbrain 14 ± 9%, thalamus 11 ± 3%, and hypothalamus 12 ± 2%. Figure S1d). Of note, receptor expression within the hippocampus was similar throughout different hippocampal structures (Figure S1e). We also observed differences in astrocytic and neuronal receptor expression, with higher fluorescence intensity detected from the somata of hippocampal neurons (Figure 1a,b). In astrocytes, 5-HT₄R was expressed on both somata and astrocytic protrusions, although the receptor distribution was heterogeneous, with several protrusions lacking receptor expression (Figure 1d).

To acquire more detailed information regarding 5-HT₄R distribution, we also performed STED imaging of S100 β -positive astrocytes in fixed hippocampal slices. STED microscopy revealed that 5-HT₄R appeared to form separated clusters with a mean size of 136 \pm 21 nm (Figure 1e,f).

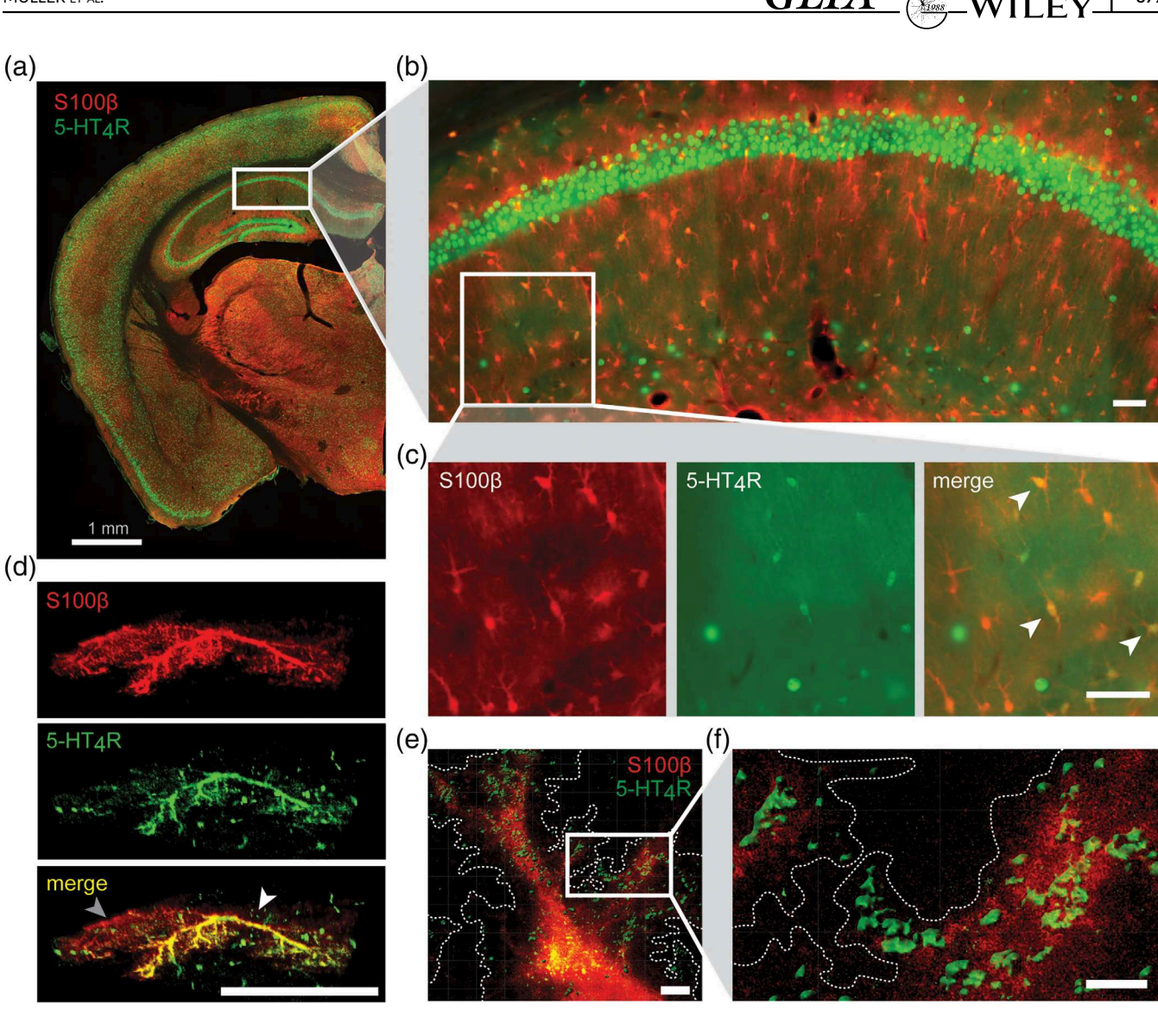


FIGURE 1 Astrocytes express the 5-HT₄R in vivo. (a) Expression of the 5-HT₄R in S100 β -positive cells throughout the mouse brain shown by immunohistochemical staining. (b) Magnification of hippocampal structures shown in (a) revealed expression of the 5-HT₄R in hippocampal astrocytes. Scale bar 50 μm. (c) Split channels for indicated area in (b). White arrows exemplarily point to 5-HT₄R expressing astrocytes. Scale bar 50 μm. (d) 3D representation of a hippocampal astrocyte visualized by S100 β and 5-HT₄R staining. 5-HT₄R was heterogeneously distributed. The grey arrow points towards a branch with less 5-HT₄R staining than the one marked by the white arrow. Scale bar 50 μm. (e) STED microscopy images showed clustering of 5-HT₄R on S100 β -positive cells. The dotted white line represents the astrocyte outline identified by S100 β labeling. Scale bar 2 μm. (f) Magnification of an astrocyte process shown in (e). Scale bar 1 μm [Color figure can be viewed at wileyonlinelibrary.com]

3.2 | Cultured hippocampal astrocytes are a suitable model for investigating 5-HT₄R-signaling

After demonstrating 5-HT_4R expression in hippocampal astrocytes in vivo, we next investigated the role of 5-HT_4R -mediated signaling in the regulation of astrocytic morphology and function. As a model system, we utilized mouse primary hippocampal astrocyte cultures, raising stellate astrocytes (Wu et al., 2014).

To verify the astrocyte enrichment in our preparation, we determined the proportions of astrocytes, neurons, and other cell types (Figure S2e). The astrocyte cultures contained 85 \pm 4% GFAP-positive cells, 3 \pm 2% neurons (as assessed by β III-tubulin expression), and

 $12\pm3\%$ other cells identified by DAPI nuclei staining. Astrocyte cultures from 5-HT₄R-ko mice showed a similar composition (78 \pm 16% GFAP⁺, 5 \pm 4% β III-tubulin⁺, and 18 \pm 13% other cells). Interestingly, the mixed hippocampal cell cultures (HCC) comprised a comparable percentage of astrocytes (87 \pm 2%), but an increased relative percentage of neurons (9 \pm 2%) and a lower proportion of cells that were not GFAP⁺ or β III-tubulin⁺ (4 \pm 2%).

Astrocytes can show an altered protein expression profile in vitro depending on the culture model used (Hertz, Chen, & Song, 2017); therefore, we first confirmed the presence of 5-HT₄R on the cultured cells. The cultured astrocytes showed pronounced 5-HT₄R expression (Figure 2a,b). Additionally, antibody specificity was verified using

10981136, 2021, 4, Downloaded from https://onlinelibrary.wiley.com/doi/10.1002/glia.23933 by Deutsches Zentrum Für Neurodeg. Wiley Online Library on [11/05/2023]. See the Terms and Conditions (https://onlinelibrary.wiley.com/nerms

-and-conditions) on Wiley Online Library for rules of use; OA articles are governed by the applicable Creative Commons Licenses

several approaches, including pre-treatment with the corresponding blocking peptide, and the staining of astrocytes isolated from 5-HT₄R-ko mice (Figures 2a,b and S2a,d). We also assessed the intracellular distribution of 5-HT₄R in cultured astrocytes and found a high degree of co-localization with

markers for the plasma membrane (i.e., PMCA) and the endoplasmatic reticulum (i.e., Calreticulin), while there was only partial co-localization with the Golgi marker (i.e., TGN38) and no evidence for co-localization with the lysosomal marker Lamp-1 (Figure S2b,c).

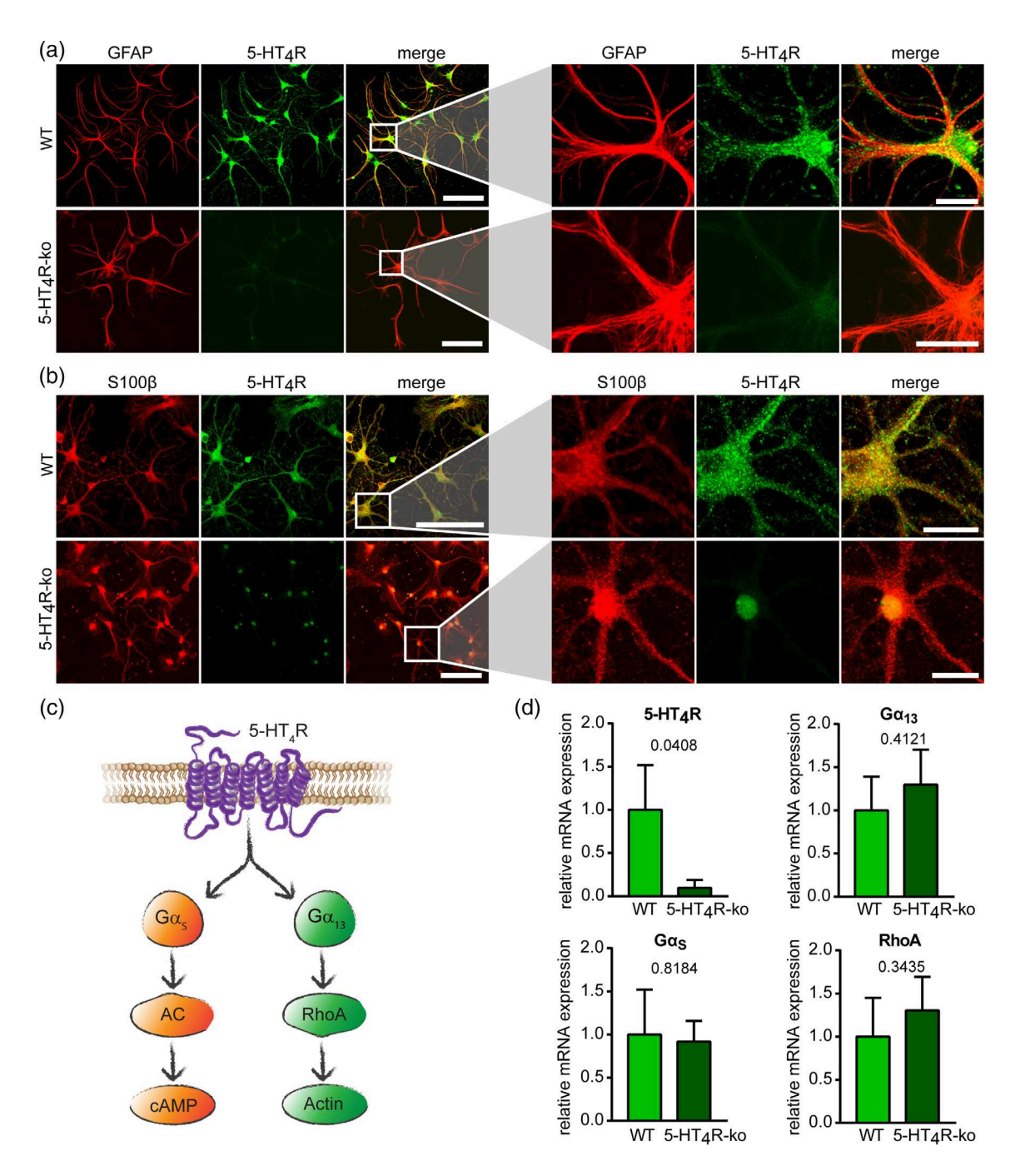


FIGURE 2 Cultured astrocytes as a model to investigate 5-HT₄R signaling. (a) Immunocytochemical labeling of 5-HT₄R astrocyte marker GFAP-positive cells in primary hippocampal cultures from WT mice. No signal of the 5-HT₄R was detected in astrocytes from 5-HT₄R-ko animals. (b) Visualization of 5-HT₄R and S100 β protein in cultured astrocytes from WT and 5-HT₄R-ko mice. Scale bars in (a) and (b) 50 μ m (left overview) and 20 μ m (right magnification). (c) Schematic illustration of established 5-HT₄R signaling pathways. Upon activation, the 5-HT₄R induced signaling via $G\alpha_S$ or $G\alpha_{13}$ heterotrimeric G proteins, leading to cAMP upregulation via adenylyl cyclase (AC) or RhoA activation and subsequent actin cytoskeleton reorganization, respectively. (d) Relative mRNA expression levels of 5-HT₄R and its down-stream effectors in primary hippocampal astrocyte cultures from WT and 5-HT₄R-ko mice. Statistical significance was evaluated using unpaired two-tailed t test, N = 4 independent cultures [Color figure can be viewed at wileyonlinelibrary.com]

19981136, 2021, 4, Downloaded from https://onlinelibrary.wiley.com/doi/10.1002/glia.2993 by Deutsches Zentrum Für Neurodeg, Wiley Online Library on [1/05/2023]. See the Terms and Conditions (https://onlinelibrary.wiley.com/terms-and-conditions) on Wiley Online Library for rules of use; OA articles are governed by the applicable Creative Commons License

As described above, 5-HT₄R couples with the $G\alpha_S$ and $G\alpha_{13}$ heterotrimeric G proteins, thereby regulating cAMP levels and modulating the conformation of the actin cytoskeleton, respectively

(Figure 2c). To ensure that the proteins involved in $5-HT_4R$ -mediated signaling were also available in the cultured hippocampal astrocytes, we performed RT-qPCR and western blot analysis. Both methods

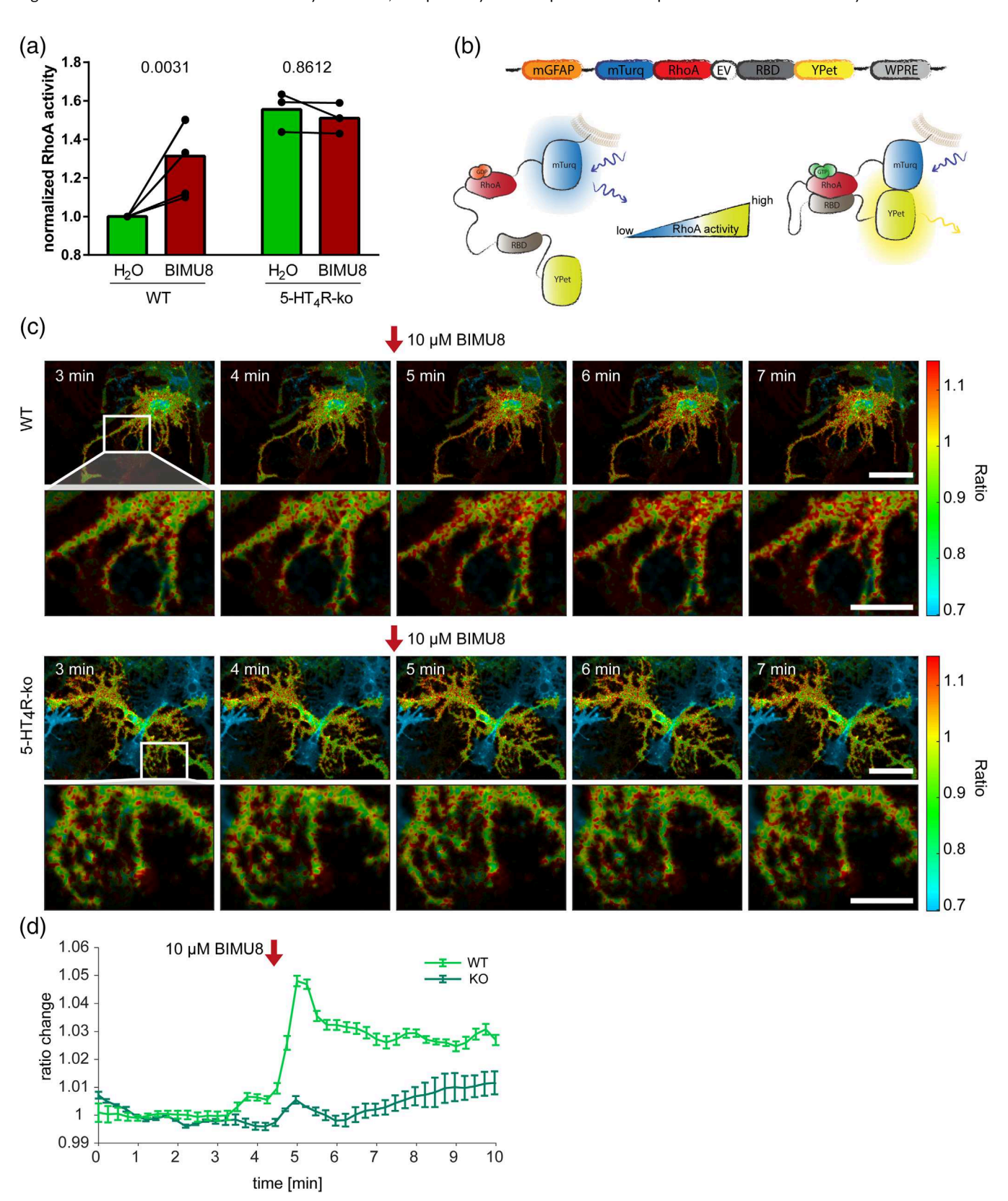


FIGURE 3 Legend on next page.

confirmed the expressions of 5-HT₄R, $G\alpha_S$, $G\alpha_{13}$, and the small GTPase RhoA in the cultured astrocytes. Importantly, astrocytic cultures isolated from 5-HT₄R-ko mice exhibited no differences in the expression levels of $G\alpha_S$, $G\alpha_{13}$, or RhoA (Figure 2d).

3.3 | 5-HT₄R activation increases RhoA activity

To investigate the impact of 5-HT_4R on astrocyte morphology, we focused on the $5\text{-HT}_4R\text{-}G\alpha_{13}\text{-}RhoA$ -actin signaling axis, which is a known regulator of cellular morphology (Kvachnina, 2005). We investigated whether this signaling pathway was preserved in hippocampal astrocytes using an ELISA-based RhoA activation assay. As shown in Figure 3a, cell treatment with the $5\text{-}HT_4R$ -selective agonist BIMU8 resulted in significantly increased RhoA activity compared with the H_2O -treated control. This increase was not detected in astrocytes isolated from $5\text{-}HT_4R$ -ko mice. Interestingly, the basal RhoA activity in $5\text{-}HT_4R$ -deficient astrocytes was 1.6-fold higher than in astrocytes isolated from the hippocampus of WT animals (Figure 3a).

We then used the FRET-based biosensor RaichuEV-RhoA to monitor 5-HT₄R-mediated RhoA activation in living cells (Figure 3b). Applying live-cell confocal imaging combined with FRET analysis, we investigated the spatiotemporal distribution of RhoA activity mediated by 5-HT₄R stimulation with BIMU8. Figure 3c depicts the time course of changes in the acceptor/donor ratio (i.e., RhoA activation) of WT and 5-HT₄R-deficient astrocytes following BIMU8 treatment. Quantitative analysis revealed a significant transient increase of the acceptor/donor ratio in WT cells, which was observed 1 min after agonist application and persisted for at least 5 min (Figure 3d). This increase was not observed after BIMU8 treatment of astrocytes isolated from 5-HT₄R-ko mice (Figure 3c,d). Overall, these findings demonstrated that 5-HT₄R activation resulted in transient and selective RhoA activation in astrocytes.

3.4 | 5-HT₄R-mediated signaling regulates actin cytoskeleton reorganization in astrocytes

RhoA activity plays a key role in actin cytoskeleton reorganization. To examine whether 5-HT₄R-induced RhoA activation modulated actin filament dynamics, we compared the ratio of filamentous actin (F-actin) to globular actin (G-actin) in astrocytes isolated from WT and 5-HT₄R-ko

mice. F-actin and G-actin were visualized by staining astrocytes with phalloidin-TRITC and DNase I-Alexa Fluor 488, respectively. Based on the ratiometric overlay of F-actin and G-actin emissions, we visualized the F-actin fraction, which ranged from 0 (low F-actin, high G-actin) to 1 (high F-actin, low G-actin) (Figure 4a). WT astrocytes treated with BIMU8 for 30 min exhibited a significant increase of the F- to G-actin ratio, from 1.6 ± 0.7 in control cells to 3.1 ± 1.3 in BIMU8-treated astrocytes (Figure 4b). This effect was 5-HT₄R-specific, as it did not occur in astrocytes from 5-HT₄R-ko mice. Furthermore, astrocytes from 5-HT₄R-ko mice exhibited a higher basal F-actin to G-actin ratio (2.5 ± 0.9 in control cells, and 2.2 ± 0.9 after BIMU8 treatment) (Figure 4a,b).

Border-distance plots provided further information about the cellular distribution of F- and G-actin. Figure 4c shows the intensity distributions of F- and G-actin structures, as well as the F-actin to G-actin fraction, in WT and 5-HT₄R-ko astrocytes as a function of distance from the cell border. Astrocyte treatment with BIMU8 increased the F-actin fraction in WT astrocytes, with the highest values observed near the plasma membrane. Comparison of F-actin and G-actin intensities revealed that the increased F-actin fraction was due to an increased F-actin level rather than a decrease of G-actin signal. In non-stimulated cells, we observed more F-actin than G-actin structures near the plasma membrane, and more G-actin than F-actin structures toward the cell center. In contrast, 5-HT₄R-deficient astrocytes exhibited a higher F-actin fraction throughout the whole cell at baseline, and no change in the F-actin fraction upon BIMU8 treatment (Figure 4c). Examination of astrocytic morphology by Sholl analysis revealed that BIMU8 treatment reduced arborization complexity (Figure 4d), indicating a general retraction of astrocytic protrusions upon 5-HT₄R activation (see also greycolor contour image inset in Figure 4a).

In summary, our results indicated that 5-HT₄R-mediated signaling in astrocytes resulted in an increased relative abundance of filamentous actin, and thereby influenced cell morphology.

$3.5 \mid 5\text{-HT}_4R$ signaling in astrocytes is G protein-dependent

As mentioned above, 5-HT₄R can activate both $G\alpha_{13}$ and $G\alpha_{5}$ proteins; thus, we next aimed to determine which G protein primarily

FIGURE 3 5-HT₄R stimulation leads to RhoA activation. (a) RhoA activity determined by RhoA activation assay in primary astrocyte cultures from WT and 5-HT₄R-ko mice after 5 min stimulation with 5-HT₄R-agonist BIMU8 or H₂O (control). WT astrocytes showed higher RhoA activity when treated with BIMU8 compared with H₂O treated cells, while 5-HT₄R-ko astrocytes displayed higher basal RhoA activity which was not changed upon BIMU8 application. Statistical significance was calculated using two-way ANOVA with Sidak's multiple comparisons post hoc test, N = 6 (WT) and N = 3 (5-HT₄R-ko) independent cultures. (b) Schematic overview of the AAV-construct containing FRET-based biosensor RaichuEV-RhoA under control of mGFAP promoter and graphic illustration of the biosensor. Upon RhoA activation both fluorophores (mTurquoise and YPet) come into close proximity and FRET occurs. (c) Time series of FRET-based biosensor RaichuEV-RhoA expressed in AAV-infected hippocampal astrocytes. Application of 5-HT₄R agonist BIMU8 after 4.5 min of recording led to a rapid increase in YPet/mTurquoise fluorescence intensity ratio of the sensor, reflecting RhoA activation. Representative from n = 139 cells for WT and from n = 12 cells for 5-HT₄R-KO. Scale bars 20 μm. (d) Time traces of selected representative cells shown in (c) depict a rapid ratio change upon 5-HT₄R stimulation with BIMU8 in WT but not 5-HT₄R-ko astrocytes. Statistical analysis using Wilcoxon matched-pairs signed rank test (p < .0001 for WT, n = 139 cells and p = .1763 for 5-HT₄R-KO, n = 12 cells) [Color figure can be viewed at wileyonlinelibrary.com]

0981135, 2021, 4, Downloaded from https://onlinelibarry.wiley.com/doi/10.1002/glia.23933 by Deutsches Zatrunt Für Neurodeg, Wiley Online Library on [11/05/2023]. See the Terms and Conditions (https://onlinelibrary.wiley.com/nerms-and-conditions) on Wiley Online Library for rules of use; OA articles are governed by the applicable Creative Commons Licenseque (11/05/2023). See the Terms and Conditions (https://onlinelibrary.wiley.com/nerms-and-conditions) on Wiley Online Library for rules of use; OA articles are governed by the applicable Creative Commons Licenseque (11/05/2023). See the Terms and Conditions (https://onlinelibrary.wiley.com/nerms-and-conditions) on Wiley Online Library for rules of use; OA articles are governed by the applicable (11/05/2023).

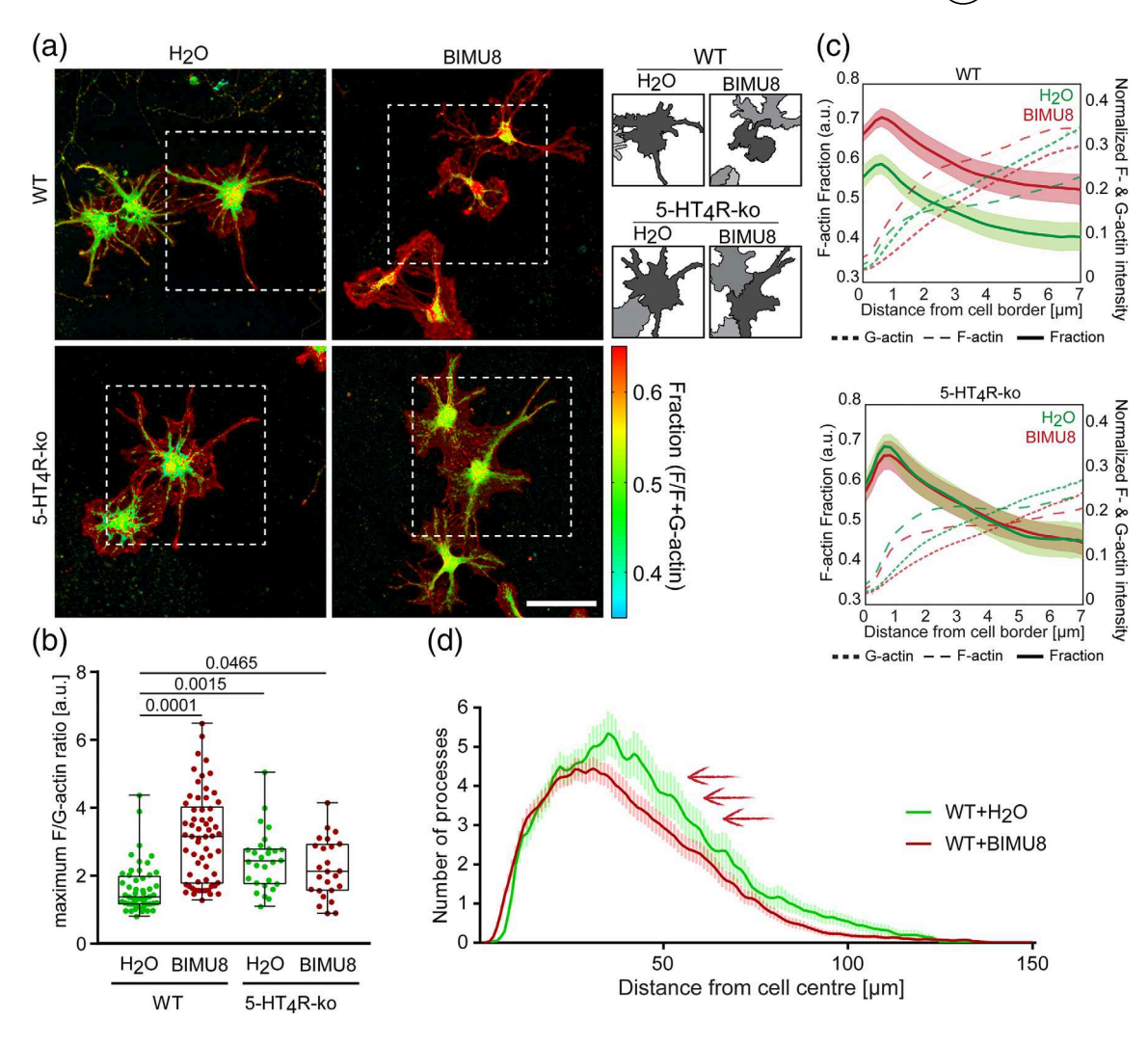


FIGURE 4 5-HT₄R-activation leads to actin reorganization. (a) Representative images showing F-actin fraction in fixed hippocampal astrocytes. In WT astrocytes the stimulation with BIMU8 (30 min, 10 μM) resulted in an increase in the F-actin fraction. In 5-HT₄R-ko astrocytes the initial fraction was higher and addition of BIMU8 had no effect. The cells from the excerpts indicated by white boxes are additionally shown uniformly in grey color on the right, to emphasize the cell area and branching. Scale bar 20 μm. (b) The quantification reflected an increase in the F- to G-actin ratio upon BIMU8 treatment in WT but not in 5-HT₄R-ko astrocytes. Statistical differences were calculated using one-way ANOVA with Dunnett's multiple comparisons post hoc test, $n \ge 25$ cells, N = 3. (c) Border-distance plots indicate the gradient of F- and G-actin intensities from the outer cell border to the center with a proportional shift upon BIMU8 treatment in WT (upper plot) but not in 5-HT₄R-ko astrocytes (lower plot), $n \ge 25$ cells, N = 3. (d) Sholl analysis reflected a reduction in arborization complexity in BIMU8 treated astrocytes (Area under the curve [AUC] 224 ± 15) compared with control cells (AUC 270 ± 15). Unpaired t-test with Welch's correction, p = .038, $n \ge 31$ cells, N = 3. Arrows point towards direction of change [Color figure can be viewed at wileyonlinelibrary.com]

participated in the 5-HT₄R-mediated reorganization of the actin cyto-skeleton in astrocytes. We developed short hairpin RNAs (shRNAs) to silence endogenously expressed $G\alpha_{13}$ or $G\alpha_S$ subunits (Figure S3a), and infected cultured astrocytes with AAVs encoding these shRNAs or scrambled shRNA as control. At 5 days after infection, real-time PCR analyses confirmed that $G\alpha_{13}$ -silenced and $G\alpha_S$ -silenced astrocytes exhibited reduced expressions of $G\alpha_{13}$ and $G\alpha_S$ mRNA, respectively: $12.6 \pm 3\%$ and $8.0 \pm 3\%$ compared with scrambled shRNA control cells (Figure S3b). Specificity of shRNAs was further confirmed by western blot analysis, which revealed efficient downregulation of protein expression without cross-reactivity or modulation of

expression of other G protein subunits, including $G\alpha_i$, $G\alpha_{12}$, and $G\alpha_q$ (36.4 ± 5% of control for $G\alpha_{13}$, and 35 ± 9% of control for $G\alpha_S$) (Figure S3c-e). Following validation, these shRNAs were used to investigate the impacts of $G\alpha_{13}$ and $G\alpha_S$ on F-actin and G-actin dynamics.

The silencing of $G\alpha_{13}$ protein in astrocytes significantly increased the F-actin fraction without 5-HT₄R stimulation, while silencing of $G\alpha_S$ did not influence the basal actin cytoskeleton composition (Figure 5a,b). Similar to control cells, $G\alpha_S$ -deficient astrocytes exhibited a significantly increased F-actin fraction following treatment with the 5-HT₄R agonist BIMU8 (Figure 5a,b). In contrast, in $G\alpha_{13}$ -

1098113, 2021, 4, Downloaded from https://onlinelibrary.wiley.com/doi/10.1002/gita.2933 by Deutsches Zentrum Für Neurodeg, Wiley Online Library on [1105/2023]. See the Terms and Conditions (https://onlinelibrary.wiley.com/nerms-and-conditions) on Wiley Online Library for rules of use; OA articles are governed by the applicable Creative Commons Licensea.

deficient astrocytes, which exhibited a high basal F-actin fraction, receptor stimulation with BIMU8 induced a significant reduction of filamentous actin (Figure 5a,b). These findings indicated a balance

between $G\alpha_S$ and $G\alpha_{13}$ protein-mediated signaling under basal conditions, and upon 5-HT₄R activation, which exerted a bidirectional influence on the actin cytoskeleton in astrocytes.

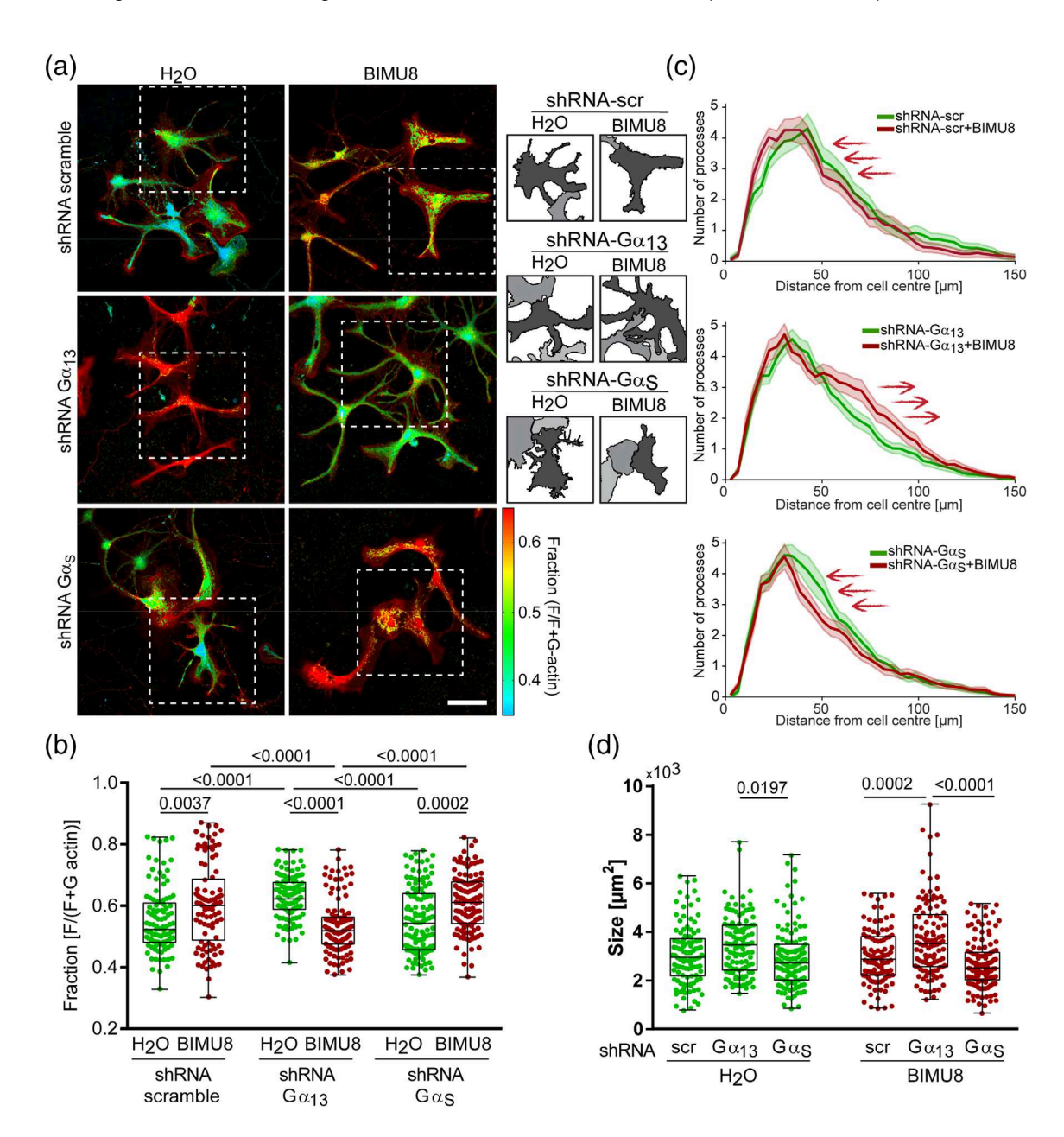


FIGURE 5 Impact of 5-HT₄R activation on the actin cytoskeleton is G protein dependent. (a) Representative images showing F-actin fraction in cultured hippocampal astrocytes infected with AAVs encoding shRNA scramble, shRNA against $G\alpha_{13}$ or shRNA against $G\alpha_{5}$ proteins. Stimulation with 5-HT₄R agonist BIMU8 (30 min, 10 μ M) increased the F-actin fraction under control conditions as well as in cells expressing less $G\alpha_{5}$. If $G\alpha_{13}$ expression was downregulated, this effect was reversed and stimulation of the receptor led to restoration of levels similar to the control. The cells from the excerpts indicated by white boxes are additionally shown uniformly in grey color on the right, to emphasize the cell area and branching. Scale bar 20 μ m. (b) Quantification of the F-actin fraction. Statistical differences were calculated using two-way ANOVA with Tukey's multiple comparisons post hoc test, $n \ge 101$ cells, N = 3. (c) Sholl analysis revealed a reduction in astrocyte complexity upon BIMU8 stimulation. Knockdown of $G\alpha_{5}$ by shRNA enhanced this effect, while stimulation had the opposite effect in astrocytes with downregulated $G\alpha_{13}$ protein levels, leading to increased complexity. Two-way ANOVA with Tukey's multiple comparisons test. shRNA-scr and shRNA-scr + BIMU8: radius 18 μ m p = .0195; shRNA- $G\alpha_{13}$ and shRNA- $G\alpha_{13}$ + BIMU8: radius 70 μ m p = .0045; shRNA- $G\alpha_{5}$ and shRNA- $G\alpha_{5}$ + BIMU8: radius 46 μ m p = .0007; $n \ge 25$ cells, N = 3. Arrows point out direction of change upon BIMU8 treatment. (d) Quantification of astrocyte size (2D) showed the impact of G protein signaling in regulation of cell size. Astrocytes occupied more space when expressing shRNA against $G\alpha_{13}$ compared with astrocytes expressing shRNA against $G\alpha_{5}$. This difference was more prominent upon stimulation with 5-HT₄R agonist BIMU8. Statistical differences were calculated using two-way ANOVA with Tukey's multiple comparisons post hoc test, $n \ge 98$ cells, N = 3 [Color figure can be view

0981136, 2021 , 4, Downloaded from https://onlinelibrary.wiley.com/doi/10.1002/glia.23933 by Deutsches Zentrum Für Neurodeg, Wiley Online Library on [11/05/2023]. See the Terms and Conditions (https://onlinelibrary.wiley.com/nerms -and-conditions) on Wiley Online Library for rules of use; OA articles are governed by the applicable Creative Commons License

We further performed Sholl analysis to confirm the dual role of $G\alpha_S$ and $G\alpha_{13}$ in regulating astrocytic morphology. At 30 min after treatment with BIMU8, astrocytes expressing shRNA-scramble or shRNA against Gas showed reduced arborization complexity (Figure 5c). In contrast, in astrocytes with downregulated $G\alpha_{13}$, BIMU8 treatment led to increased morphological complexity and an altered cell size. Under basal conditions, astrocytes expressing shRNA against $G\alpha_{13}$ were larger than astrocytes expressing shRNA against $G\alpha_S$ (0.206 ± 0.007 mm² vs. 0.172 ± 0.007 mm²). These size differences were even more pronounced after 5-HT₄R stimulation with BIMU8 $(0.224 \pm 0.009 \text{ mm}^2 \text{ vs. } 0.158 \pm 0.005 \text{ mm}^2; \text{ Figure 5d, see}$ also grey-color contour image inset in Figure 5a). To further confirm these effects to be directly mediated by the $G\alpha_{13}$ -RhoA signaling axis, we repeated these experiments in presence of Y-27632, a cell-permeable, highly potent, and selective inhibitor of the RhoA downstream effector Rho associated kinase (ROCK) (Figure S4). In the presence of this ROCK inhibitor, the 5-HT₄R agonist BIMU8 failed to change the relative F-actin fraction (Figure S4a,b) and the branching pattern of astrocytic processes (Figure S4c,d). This indicates that ROCK mediates the overall effect of 5-HT₄R activation on both.

Taken together, the emerging picture is that activation of astrocytic 5-HT₄R increases RhoA activity (Figure 3), which increases the relative abundance of F- over G-actin (Figure 4) and decreases the arborization of astrocytes (Figure 5) via ROCK signaling (Figure S4). Although 5-HT₄R signaling can be mediated by both $G\alpha_{13}$ and $G\alpha_{S}$, the overall effect of receptor activation is dominated by the action of $G\alpha_{13}$ (Figure 5). In addition, the observation of increased basal RhoA activity (Figure 3a) and relative F-actin levels (Figure 4b) in 5-HT₄R knockout astrocytes indicates that in the absence of this receptor alternative signaling pathways can gain increased control over the cytoskeleton (see also Figures S4e,f and S7).

3.6 | 5-HT₄R activation in astrocytes changes excitatory synaptic transmission in vitro and in situ

Activation of 5-HT₄R reportedly causes a long-lasting increase in the excitability of hippocampal neurons (Mlinar, Mascalchi, Mannaioni, Morini, & Corradetti, 2006), converts a weak synaptic potentiation into persistent LTP in the CA1 area (Matsumoto et al., 2001) and directly potentiate CA3-CA1 synapses (Teixeira et al., 2018). Since astrocytes and neurons are both involved in regulating multiple brain functions, including synaptic transmission, it is crucial to understand whether 5-HT₄R activation in astrocytes could have functional consequences on the neuronal network. To investigate the possible role of astrocytic 5-HT₄R on synaptic activity, we prepared primary hippocampal mixed cultures from 5-HT₄R-ko mice. In these cultures, we selectively rescued 5-HT₄R expression in either neurons or astrocytes, using AAV vectors encoding 5-HT₄R under control of a synapsin or GFAP promoter, respectively. The control cell cultures were infected with AAVs encoding tdTomato under control of a synapsin or GFAP promoter (Figures 6a and S5a). We verified the selective 5-HT₄R expression in neurons or astrocytes by immunofluorescence staining with antibodies against GFAP (astrocytic marker) or β III-tubulin (neuronal marker), respectively (Figure S5b). Whole-cell patch-clamp recordings were obtained from cultured neurons to compare the influence of 5-HT₄R activation on mEPSCs between those conditions.

In the control condition (5-HT₄R-ko cultures expressing tdTomato), application of BIMU8 did not change the mEPSC frequency (Figure 6a,b). Receptor stimulation with BIMU8 also did not change the mEPSC frequency in cells with selective rescue of neuronal 5-HT₄R expression (Figure 6a,b). In contrast, 5HT₄R activation induced a significantly increased mEPSC frequency within minutes in cells with selective rescue of 5-HT₄R expression in astrocytes (Figure 6a,b). To determine whether this effect was mediated via the 5-HT₄R-Gα₁₃-RhoA-ROCK signaling pathway, we performed electrophysiological recordings in the presence of the ROCK inhibitor Y-27632. Although Y-27632 affects RhoA signaling in both neurons and astrocytes, our observation, that the selective rescue of 5-HT₄R expression in neurons did not influence BIMU8-mediated changes in mEPSC (Figure 6b), demonstrates that the 5-HT₄R-RhoA-ROCK signaling in neurons is not implemented in BIMU8-mediated EPSC frequency response. Therefore, the effect of Y-27632 was analyzed only in cultures where 5-HT₄R expression was selectively rescued in astrocytes. In these experiments, no increase of the mEPSC frequency was observed after BIMU8 stimulation in 5-HT₄R expressing astrocyte cultures (Figure 6b). We observed a nonspecific rundown of mEPSC amplitudes, which was present in all groups to the same extent. These results suggest that astrocytic 5-HT₄R modulated an increase of spontaneous neurotransmitter release at glutamatergic synapses in cultured cells mediated by the 5-HT₄R-G α ₁₃-RhoA-ROCK signaling.

Finally, we examined the role of astrocytic 5-HT₄R in glutamatergic synaptic transmission in the hippocampus in situ. To this end, we stereotactically injected 5-HT₄R-ko mice in the hippocampal CA1 region of one hemisphere with a control AAV-GFAP-tdTomato construct. Each mouse was also injected in the CA1 hippocampus of the other hemisphere with AAV-GFAP-5-HT₄R-eGFP to selectively rescue astrocytic 5-HT₄R expression (Figure 7a and S6a-c). Three weeks after stereotactic injection, acute hippocampal slices were prepared. AAV-mediated rescue of 5-HT₄R expression resulted in a heterogeneous expression pattern similar to that obtained for the endogenous receptor (Figure S6d). We identified the slices containing transfected astrocytes using two-photon excitation fluorescence microscopy (Figure 7b). Next, fEPSPs were evoked by electrical stimulation of CA3-CA1 Schaffer collateral axons and recorded in the CA1 stratum radiatum near astrocytes expressing either 5-HT₄R-eGFP (rescue) or tdTomato (knockout). Basal synaptic transmission did not differ between the rescue and knockout slices (Figure 7c), and the fEPSP slope was not affected by bath application of 10 μM BIMU8 for 20 min (fEPSP slope normalized to pre-drug baseline: knockout, 99.7 \pm 2.93%, n = 6, p = .919; rescue, 97.7 \pm 4.88%, p = .658, n = 8; paired t-tests; not illustrated). However, the paired-pulse-ratio (PPR) at short inter-stimulus intervals of 25 ms was significantly reduced in slices with rescued astrocytic 5-HT₄R expression compared with control slices (Figure 7d). Thus, the selective rescue of 5-HT₄R expression in astrocytes affected glutamate release at these synapses. Again, the

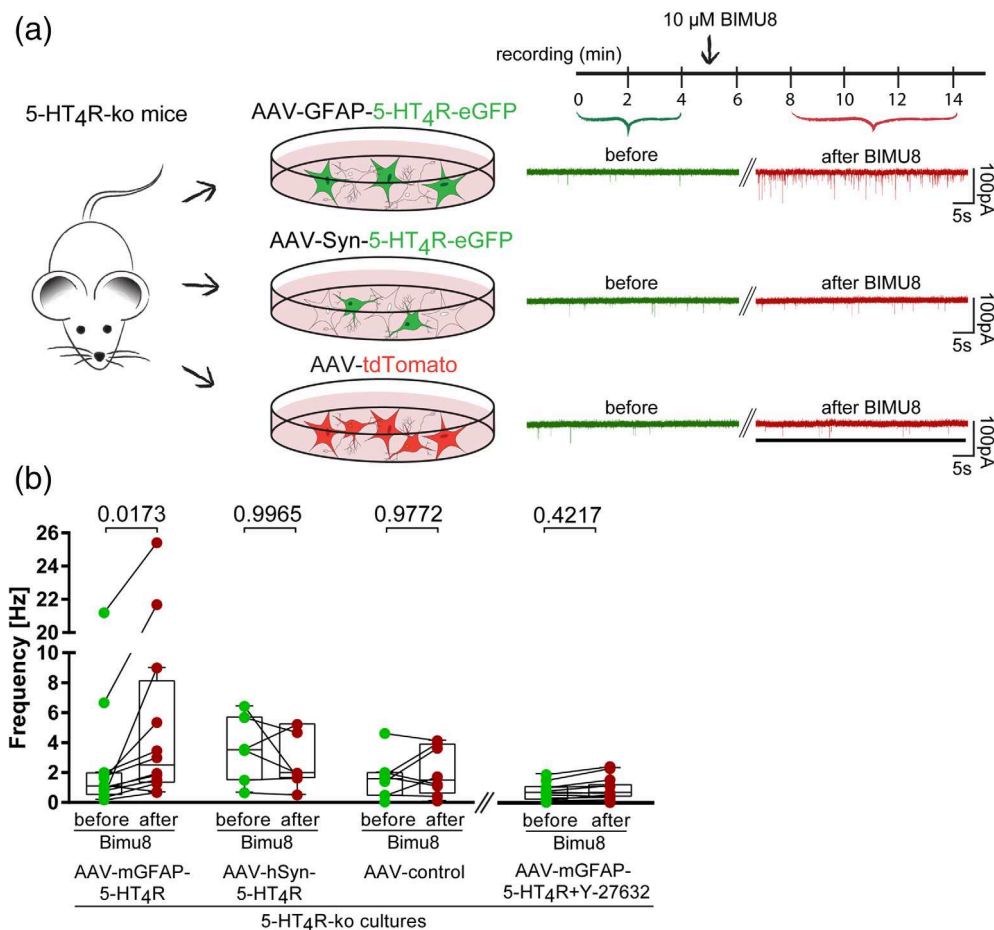


FIGURE 6 5-HT₄R activation in astrocytes impacts neuronal signaling. (a) Illustration of the experimental setup with three conditions. 5-HT₄R-ko mice were used for preparation of mixed hippocampal cultures (HCC) and the receptor was either rescued in astrocytes or neurons using viral infection of AAV-mGFAP-5-HT₄R-eGFP or AAV-syn-5-HT₄R-eGFP, respectively. In a third (control) condition cells were infected with AAV-tdTomato. Representative traces of electrophysiological recordings of neurons in those cultures are shown on the right for all three conditions. Only rescued expression of the 5-HT₄R in astrocytes, but not neurons, influenced mEPSC frequency after BIMU8 stimulation. (b) Quantification of mEPSC frequency in hippocampal neurons after application of 10 μM 5-HT₄R agonist BIMU8. Increase of mEPSC frequency was only present if astrocytes expressed 5-HT₄Rs, but not if the receptor was only present in neurons. No change was observed upon BIMU8 stimulation in a 5-HT₄R-ko culture or when RhoA signaling was blocked by cell-permeable, highly potent ROCK inhibitor Y-27632 (50 μM). Statistical analysis was performed using two-way ANOVA with Sidak's multiple comparisons post hoc test, $n \ge 7$ [Color figure can be viewed at wileyonlinelibrary.com]

rescue of 5-HT₄R had no effect when recordings were performed in the presence of the ROCK inhibitor Y-27632 (Figure 7e,f). Together our electrophysiological experiments indicate that astrocytic 5-HT₄Rs modulate presynaptic glutamate release in cultures and acute slices via signaling of ROCK.

DISCUSSION

The role of serotonergic signaling in the brain has been extensively studied over the last decades. However, such research has been largely focused on the impact of serotonin receptors on neurons. As increasing evidence highlights the importance of astrocytes in regulating physiological brain functions and in many neurological disorders, these cells must be considered important contributors to diseases involving serotonergic signaling changes (Lundgaard, Osório, Kress,

Sanggaard, & Nedergaard, 2014; Miyazaki & Asanuma, 2016; Peng, Verkhratsky, Gu, & Li, 2015). Moreover, astrocytes represent an essential part of the multipartite synapse. Thus, the expression of serotonin receptors on astrocytes in brain regions with serotonergic innervation might represent an important, yet largely unexplored, signaling pathway.

Our present findings confirmed the astrocytic expression of 5-HT₄R (Boisvert et al., 2018; Cahoy et al., 2008; Parga et al., 2007) and demonstrated that this receptor was expressed on a subset of astrocytes. These observations are in line with multiple studies revealing astrocyte heterogeneity in terms of morphology and function (Farmer & Murai, 2017; Matyash & Kettenmann, 2010; Oberheim, Goldman, & Nedergaard, 2012). The distinct expression pattern may also result from the defined structures of serotonergic projections within the hippocampus. Moreover, we observed irregular and clustered distributions of 5-HT₄R within single astrocytes, which could be

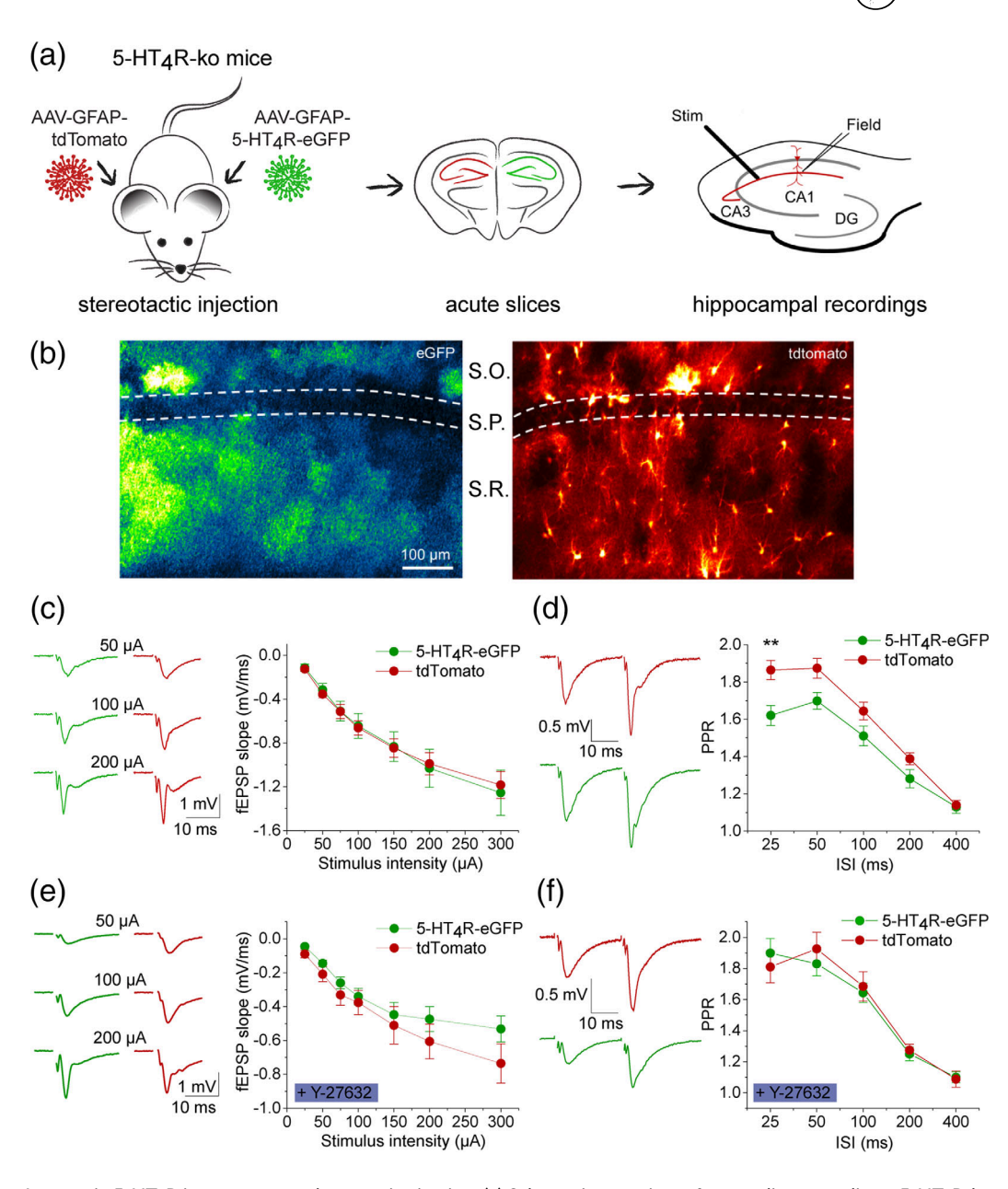


FIGURE 7 Astrocytic 5-HT₄R impact neuronal properties in vivo. (a) Schematic overview of acute slice recordings. 5-HT₄R-ko mice were stereotactically injected with AAV-GFAP-5-HT₄R-eGFP and AAV-GFAP-tdTomato into separate hemispheres to selectively restore astroglial 5-HT₄Rs in the hippocampus. After 3 weeks acute slices were subjected to electrophysiological investigations. fEPSPs were evoked by electrical stimulation of CA3-CA1 Schaffer collaterals and recorded in the stratum radiatum (S.R.) of the CA1 region. (b) Astroglial expression of AAVs was visualized using two-photon excitation fluorescence microscopy. Transfected astrocytes were uniformly distributed across stratum oriens (S.O.) and S.R. Unlike cytosolic tdTomato the 5-HT₄R-eGFP fusion protein was located to astrocytic membranes. Stratum pyramidale (S.P.) indicated for orientation. (c) Representative fEPSPs recorded in S.R. with gradually increasing stimulation intensities (left panel, examples for 50, 100, 200 µA). fEPSP slopes recorded near 5-HT₄R-eGFP expressing astrocytes (green) or areas covered by tdTomato expressing astrocytes (red) were not statistically different (right panel, p = .87, two-way repeated measures ANOVA, eGFP n = 11, tdTomato n = 14). (d) Representative pairs of fEPSPs recorded with an inter-stimulus interval of 25 ms (left panel). The paired-pulse ratio (PPR) obtained at short inter-stimulus intervals (ISI) was lower when astroglial 5-HT₄R expression was rescued compared with tdTomato-positive control slices (p = .0084, two-way repeated measures ANOVA, eGFP n = 10, tdTomato n = 14, Tukey post hoc test: 25 ms, p = .0065, **50 ms, p = .145). (e-f) The experiments were repeated in the presence of ROCK inhibitor Y-27632 (20 μM). The fEPSP slopes recorded near 5-HT4R-eGFP-expressing astrocytes were not significantly different from fEPSPs recorded close to tdTomato-expressing astrocytes (p = .225, two-way repeated measures ANOVA, eGFP n = 13, tdTomato n = 12). Also the PPR was not different between these conditions when ROCK was blocked (p = .873, two-way repeated measures ANOVA, eGFP n = 13, tdTomato n = 12) [Color figure can be viewed at wileyonlinelibrary.com]

temporally or structurally correlated, as recently demonstrated for the GABA transporter GAT-3 (Boddum et al., 2016; Mederos, González-Arias, & Perea, 2018). Our results indicated that activation of the 5-HT $_4$ R-G $_{13}$ signaling pathway induced activation of the small GTPase RhoA in astrocytes, which led to an increased F-actin fraction and morphological changes. The observed morphological changes could be critically involved in synapse formation, maintenance, and plasticity (Chung et al., 2015; Dallérac, Zapata, & Rouach, 2018; Haber, Zhou, & Murai, 2006).

We found that treatment with the selective 5-HT₄R agonist BIMU8 induced an increase in filamentous actin structures. Moreover, this effect was absent in 5-HT₄R-ko astrocytes, demonstrating 5-HT₄R specificity. Interestingly, cultured astrocytes from 5-HT₄Rko mice exhibited altered properties under basal conditions: elevated RhoA activity and an increased basal F-actin fraction. The same phenomenon was observed following the downregulation of $G\alpha_{13}$ proteins in astrocytes from WT mice. We propose that under basal conditions, 5-HT₄R is negatively coupled to $G\alpha_s$ and $G\alpha_{13}$ proteins, with the latter being the preferential partner (Figure S7). Upon receptor knockout, $G\alpha_{13}$ becomes disinhibited leading to activation of the RhoA cascade and increased F-actin formation. Knockingdown the $G\alpha_{13}$ subunit shifts a negative coupling of 5-HT₄R towards Gα_s, which can lead to decreased RhoA phosphorylation via cAMPdependent kinases resulting in RhoA disinhibition (see below). Receptor stimulation with an agonist activates the $G\alpha_{13}$ -RhoA signaling pathway and boosts F-actin formation (Figure S7). In case of $G\alpha_{13}$ knockdown, receptor stimulation preferentially induces a $G\alpha$ smediated rise of cAMP levels, leading to increased RhoA phosphorylation by PKA (Jaffe & Hall, 2005; Kim et al., 2018). As consequence, RhoA-mediated activation of ROCK kinase is attenuated, leading to inhibition of F-actin formation. Supporting this view, a new concept, in which Gas signaling negatively regulates guanine nucleotide exchange factors (GEFs) that are responsible for activating the small GTPases Cdc42 and Rac1 was recently presented by Sugiyama and co-workers (Sugiyama et al., 2017). Since low Cdc42 and Rac1 activity are reportedly accompanied by elevated RhoA activity (Bishop & Hall, 2000; Chauhan, Lou, Zheng, & Lang, 2011), chronic upregulation of active RhoA may account for the presently observed increase in F-actin.

As mentioned above, in astrocytes with diminished $G\alpha_{13}$ signaling, stimulation with BIMU8 drastically decreased the elevated basal F-actin to G-actin ratio, possibly via signaling through $G\alpha_S$ or G protein-independent pathways. Several possible links between $G\alpha_S$ signaling and the actin cytoskeleton have been proposed, including acute phosphorylation of RhoA at serine residue 188 by the cyclic nucleotide-dependent protein kinase A (PKA), which directly inhibits RhoA activity by enhancing its interaction with RhoGDI and its attendant withdrawal from the plasma membrane (Ellerbroek, Wennerberg, & Burridge, 2003; Forget, Desrosiers, Gingras, & Béliveau, 2002; Tkachenko et al., 2011). Additionally, RhoA phosphorylation by cAMP-dependent kinases causes decreased interaction with the effector protein Rho-associated coiled-coil-containing kinase (ROCK) (Nusser et al., 2006; Takemoto, Ishihara, Mizutani,

Kawabata, & Haga, 2015), which regulates actin dynamics and cell morphology via numerous effector proteins, including ROCK, LIM-kinases, Cofilin, F-actin, and the regulatory light chain of myosin (MLC) (Jaffe & Hall, 2005; Kim et al., 2018). Several reports describe antagonistic roles of RhoA and cAMP in regulating cellular morphology (Bandtlow, 2003; Dong, Leung, Manser, & Lim, 1998). Moreover, RhoA phosphorylation reduces ROCK interaction—without altering the interactions of other effector protein, including rhotekin, mDia-1, and protein kinase N (PKN)—thus, adding an additional switch and increasing the complexity of actin regulation (Nusser et al., 2006).

Downregulation of $G\alpha_S$ protein levels in astrocytes did not affect 5-HT₄R-mediated regulation of F-actin dynamics and cell morphology neither under basal conditions nor after receptor stimulation. Therefore, we conclude that under physiological conditions, 5-HT₄R signaling influences actin cytoskeleton composition predominantly via the $G\alpha_{13}$ -RhoA signaling pathway. Furthermore, our findings indicated that actin dynamics are in a balanced state, and that 5-HT₄R activity can bidirectionally regulate the turnover of F-actin and G-actin structures. Bidirectional control of actin structures is reportedly important for the regulation of spine morphology in hippocampal neurons, albeit through different mechanisms (Okamoto, Nagai, Miyawaki, & Hayashi, 2004). We also demonstrated that astrocyte morphology underlies the regulation of actin by serotonergic signaling, which adds a new player in the debate about regulation of astrocyte appearance (Matyash & Kettenmann, 2010; Oberheim et al., 2012; Zhou, Zuo, & Jiang, 2019).

It has been suggested that 5-HT_4R activity might affect overall network excitability (Schill et al., 2020). We investigated whether the manipulation of 5-HT_4R signaling in astrocytes affected glutamatergic synaptic transmission. In dissociated cultures, pharmacological activation of 5-HT_4Rs quickly increased the frequency of spontaneous synaptic glutamate release (mEPSCs). Because this happened on a timescale of ~ 10 min, this effect was likely due to an acute increase in the probability of spontaneous release from existing presynaptic glutamatergic terminals, and not synaptogenesis. The rapid onset of the increase was in line with the fast increase of RhoA activity after 5-HT_4R activation.

In situ, we recorded fEPSPs evoked by single stimulations of CA3-CA1 axons, and found that they were not changed by the rescue of astrocytic 5-HT₄R expression or by the acute pharmacological activation of the restored 5-HT₄Rs by BIMU8. There are at least two possible explanations for the absence of an acute effect. First, the modulation of synaptic transmission via astrocytic 5-HT₄Rs in situ may occur on a longer timescale than in vitro, for example, over hours or days. Second, 5-HT₄Rs might be fully activated by ambient serotonin in the slice preparation, which would prevent effects of direct receptor activation. The latter could indicate that astrocytic 5-HT₄Rs are already fully activated in acute slices. However, we also detected a reduced paired-pulse facilitation of synaptic transmission at short inter-stimulus intervals after rescuing astrocytic 5-HT₄R expression. Since the paired-pulse facilitation at CA3-CA1 synapses is thought to reflect changes of presynaptic glutamate

release (Debanne, Guérineau, Gähwiler, & Thompson, 1996; Dobrunz & Stevens, 1997 and references therein), this observation suggests that astrocytic 5-HT₄Rs modify presynaptic release (i.e., synapses with a high initial release probability show low paired-pulse facilitation, as in our case). This reduced paired-pulse facilitation was not due to an increase of the overall basal presynaptic release probability, because we did not observe a corresponding increase of the slope of single fEPSPs. Rather, it is likely that astrocytic 5-HT₄Rs modify rapid repetitive release. Both in situ and in vitro effects mediated by astrocytic 5-HT₄Rs were not observed when ROCK signaling was inhibited. Therefore, astrocytic 5-HT₄Rs can modify synaptic glutamate release via ROCK signaling both in dissociated cells and organized tissue, although the change of the mEPSC frequency in vitro and of the paired-pulse facilitation in situ do not point towards a specific presynaptic mechanism. Regarding the latter, it needs to be noted that viral delivery of 5HT₄R to hippocampal astrocytes does not lead to transduction of all astrocytes (Figure 7) and may not reproduce the relatively sparse endogenous 5HT₄R expression pattern (Figure S1), which could explain differences in the presynaptic effects between cultures and acute slices. Optical quantal analysis of release at single spines (Oertner, Sabatini, Nimchinsky, & Svoboda, 2002) near astrocytic processes positive and negative for 5-HT₄R could help to dissect the involved mechanism in future. In combination with pharmacology, this approach could also be useful to identify the involved signaling molecules (Alfonso Araque et al., 2014; Rusakov et al., 2014) that link astrocytic 5-HT₄R, RhoA, ROCK and presynaptic function.

ACKNOWLEDGMENT

The RaichuEV-RhoA biosensor was provided by Michiyuki Matsuda, which we greatly appreciate. This study was supported by the German Research Foundation (DFG) (PO732 to E. P., ZE994/2 to A. Z., SFB1089 B03, FOR2795, SPP1757 HE6949/1, HE6949/3 to C. H.), Lobachevsky University 5-100 academic excellence program to E.P., and SFB870 B05 to C. W. S. This manuscript is part of the PhD thesis of F. E. M. Open access funding enabled and organized by Projekt DEAL.

DATA AVAILABILITY STATEMENT

The data that supports the findings of this study are available in the supplementary material of this article

ORCID

Franziska E. Müller https://orcid.org/0000-0003-0525-0714 Laura Stopper https://orcid.org/0000-0002-9648-6222 Hristo Varbanov https://orcid.org/0000-0001-9828-8855 Svitlana Antoniuk https://orcid.org/0000-0002-8226-1866 *Valérie Compan* https://orcid.org/0000-0002-4634-2765 Frank Kirchhoff https://orcid.org/0000-0002-2324-2761 Christian Henneberger https://orcid.org/0000-0002-5391-7387 Evgeni Ponimaskin https://orcid.org/0000-0002-4570-5130 Andre Zeug https://orcid.org/0000-0001-9858-5841

REFERENCES

- Amundson, R. H., Goderie, S. K., & Kimelberg, H. K. (1992). Uptake of [3H] serotonin and [3H] glutamate by primary astrocyte cultures. II. Differences in cultures prepared from different brain regions. Glia, 6 (1), 9-18. https://doi.org/10.1002/glia.440060103
- Andriezen, W. L. (1893). The neuroglia elements in the human brain. British Medical Journal, 2(1700), 227-230. https://doi.org/10.1136/bmj.2. 1700.227
- Araque, A., Parpura, V., Sanzgiri, R. P., & Haydon, P. G. (1999). Tripartite synapses: Glia, the unacknowledged partner. Trends in Neurosciences, 22(5), 208-215. https://doi.org/10.1016/S0166-2236(98)01349-6
- Araque, A., Carmignoto, G., Haydon, P. G., Oliet, S. H. R., Robitaille, R., & Volterra, A. (2014). Gliotransmitters travel in time and space. Neuron, 81(4), 728-739. https://doi.org/10.1016/j.neuron.2014.02.007
- Bandtlow, C. E. (2003). Regeneration in the central nervous system. Experimental Gerontology, 38(1), 79-86. https://doi.org/10.1016/S0531-5565(02)00165-1
- Barthet, G., Framery, B., Gaven, F., Pellissier, L., Reiter, E., Claeysen, S., ... Dumuis, A. (2007). 5-Hydroxytryptamine4 receptor activation of the extracellular signal-regulated kinase pathway depends on Src activation but not on G protein or β -Arrestin signaling. Molecular Biology of the Cell, 18(6), 1979-1991. https://doi.org/10.1091/mbc.E06-12-1080
- Bishop, A. L., & Hall, A. (2000). Rho GTPases and their effector proteins. Biochemical Journal, 348(2), 241-255.
- Bockaert, J., Claeysen, S., Bécamel, C., Dumuis, A., & Marin, P. (2006). Neuronal 5-HT metabotropic receptors: Fine-tuning of their structure, signaling, and roles in synaptic modulation. Cell and Tissue Research, 326(2), 553-572. https://doi.org/10.1007/s00441-006-0286-1
- Boddum, K., Jensen, T. P., Magloire, V., Kristiansen, U., Rusakov, D. A., Pavlov, I., & Walker, M. C. (2016). Astrocytic GABA transporter activity modulates excitatory neurotransmission. Nature Communications, 7, 13572. https://doi.org/10.1038/ncomms13572
- Boisvert, M. M., Erikson, G. A., Shokhirev, M. N., & Allen, N. J. (2018). The aging astrocyte Transcriptome from multiple regions of the mouse brain. Cell Reports, 22(1), 269-285. https://doi.org/10.1016/j.celrep. 2017.12.039
- Cahoy, J. D., Emery, B., Kaushal, A., Foo, L. C., Zamanian, J. L., Christopherson, K. S., ... Barres, B. A. (2008). A Transcriptome database for astrocytes, neurons, and Oligodendrocytes: A new resource for understanding brain development and function. The Journal of Neuroscience, 28(1), 264-278. https://doi.org/10.1523/JNEUROSCI. 4178-07.2008
- Camandola, S. (2018). Astrocytes, emerging stars of energy homeostasis. Cell Stress, 2(10), 246-252. https://doi.org/10.15698/cst2018.10.157
- Chauhan, B. K., Lou, M., Zheng, Y., & Lang, R. A. (2011). Balanced Rac1 and RhoA activities regulate cell shape and drive invagination morphogenesis in epithelia. Proceedings of the National Academy of Sciences of the United States of America, 108(45), 18289-18294. https://doi.org/ 10.1073/pnas.1108993108
- Chung, W.-S., Allen, N. J., & Eroglu, C. (2015). Astrocytes control synapse formation, function, and elimination. Cold Spring Harbor Perspectives in Biology, 7(9), a020370. https://doi.org/10.1101/cshperspect.a020370
- Compan, V., Zhou, M., Grailhe, R., Gazzara, R. A., Martin, R., Gingrich, J., ... Hen, R. (2004). Attenuated response to stress and novelty and hypersensitivity to seizures in 5-HT4 receptor Knock-out mice. Journal of Neuroscience, 24(2), 412-419. https://doi.org/10.1523/JNEUROSCI. 2806-03.2004
- Dallérac, G., Zapata, J., & Rouach, N. (2018). Versatile control of synaptic circuits by astrocytes: Where, when and how? Nature Reviews Neuroscience, 19(12), 729-743. https://doi.org/10.1038/s41583-018-0080-6
- Debanne, D., Guérineau, N. C., Gähwiler, B. H., & Thompson, S. M. (1996). Paired-pulse facilitation and depression at unitary synapses in rat hippocampus: Quantal fluctuation affects subsequent release. The Journal

- of Physiology, 491(1), 163–176. https://doi.org/10.1113/jphysiol. 1996.sp021204
- Dobrunz, L. E., & Stevens, C. F. (1997). Heterogeneity of release probability, facilitation, and depletion at central synapses. *Neuron*, 18(6), 995–1008. https://doi.org/10.1016/s0896-6273(00)80338-4
- Dong, J.-M., Leung, T., Manser, E., & Lim, L. (1998). cAMP-induced morphological changes are counteracted by the activated RhoA small GTPase and the rho kinase ROKα. *Journal of Biological Chemistry*, 273 (35), 22554–22562. https://doi.org/10.1074/jbc.273.35.22554
- Ellerbroek, S. M., Wennerberg, K., & Burridge, K. (2003). Serine phosphorylation negatively regulates RhoA in vivo. *Journal of Biological Chemistry*, 278(21), 19023–19031. https://doi.org/10.1074/jbc. M213066200
- Farmer, W. T., & Murai, K. (2017). Resolving astrocyte heterogeneity in the CNS. Frontiers in Cellular Neuroscience, 11, 300. https://doi.org/10. 3389/fncel.2017.00300
- Flores-Méndez, M., Mendez-Flores, O. G., & Ortega, A. (2016). Glia plasma membrane transporters: Key players in glutamatergic neurotransmission. *Neurochemistry International*, 98, 46–55. https://doi.org/10. 1016/j.neuint.2016.04.004
- Forget, M.-A., Desrosiers, R. R., Gingras, D., & Béliveau, R. (2002). Phosphorylation states of Cdc42 and RhoA regulate their interactions with rho GDP dissociation inhibitor and their extraction from biological membranes. *Biochemical Journal*, 361(2), 243–254. https://doi.org/10.1042/bi3610243
- Haber, M., Zhou, L., & Murai, K. K. (2006). Cooperative astrocyte and dendritic spine dynamics at hippocampal excitatory synapses. The Journal of Neuroscience: The Official Journal of the Society for Neuroscience, 26 (35), 8881–8891. https://doi.org/10.1523/JNEUROSCI.1302-06. 2006
- Halassa, M. M., Fellin, T., Takano, H., Dong, J.-H., & Haydon, P. G. (2007). Synaptic islands defined by the territory of a single astrocyte. *The Journal of Neuroscience: The Official Journal of the Society for Neuroscience*, 27(24), 6473–6477. https://doi.org/10.1523/JNEUROSCI.1419-07. 2007
- Hall, A. (2005). Rho GTPases and the control of cell behaviour. *Biochemical Society Transactions*, 33(5), 891–895. https://doi.org/10.1042/BST20050891
- Hall, A. (1998). Rho GTPases and the Actin cytoskeleton. *Science*, *279* (5350), 509-514. https://doi.org/10.1126/science.279.5350.509
- Hertz, L., Chen, Y., & Song, D. (2017). Astrocyte cultures mimicking brain astrocytes in gene expression, signaling, metabolism and K+ uptake and showing Astrocytic gene expression overlooked by immunohistochemistry and in situ hybridization. *Neurochemical Research*, 42(1), 254–271. https://doi.org/10.1007/s11064-016-1828-x
- Jaffe, A. B., & Hall, A. (2005). RHO GTPASES: Biochemistry and Biology [Review-article]. Http://Dx.Doi.Org/10.1146/Annurev.Cellbio.21. 020604.150721. http://www.annualreviews.org/doi/abs/10.1146/annurev.cellbio.21.020604.150721
- Kim, J.-G., Islam, R., Cho, J. Y., Jeong, H., Cap, K.-C., Park, Y., ... Park, J.-B. (2018). Regulation of RhoA GTPase and various transcription factors in the RhoA pathway. *Journal of Cellular Physiology*, 233(9), 6381–6392. https://doi.org/10.1002/jcp.26487
- Kobe, F., Guseva, D., Jensen, T. P., Wirth, A., Renner, U., Hess, D., ... Ponimaskin, E. (2012). 5-HT7R/G12 signaling regulates neuronal morphology and function in an age-dependent manner. *The Journal of Neuroscience*, 32(9), 2915–2930. https://doi.org/10.1523/JNEUROSCI. 2765-11.2012
- Kvachnina, E. (2005). 5-HT7 receptor is coupled to G subunits of Heterotrimeric G12-protein to regulate gene transcription and neuronal morphology. *Journal of Neuroscience*, 25(34), 7821–7830. https://doi.org/ 10.1523/JNEUROSCI.1790-05.2005
- Lee, H. S., Ghetti, A., Pinto-Duarte, A., Wang, X., Dziewczapolski, G., Galimi, F., ... Heinemann, S. F. (2014). Astrocytes contribute to gamma oscillations and recognition memory. *Proceedings of the National*

- Academy of Sciences of the United States of America, 111(32), E3343-E3352. https://doi.org/10.1073/pnas.1410893111
- Lin, C.-C. J., Yu, K., Hatcher, A., Huang, T.-W., Lee, H. K., Carlson, J., ... Deneen, B. (2017). Identification of diverse astrocyte populations and their malignant analogs. *Nature Neuroscience*, 20(3), 396–405. https://doi.org/10.1038/nn.4493
- Lundgaard, I., Osório, M. J., Kress, B., Sanggaard, S., & Nedergaard, M. (2014). White matter astrocytes in health and disease. *Neuroscience*, 0, 161–173. https://doi.org/10.1016/j.neuroscience.2013.10.050
- Mackay, D. J. G., & Hall, A. (1998). Rho GTPases. Journal of Biological Chemistry, 273(33), 20685–20688. https://doi.org/10.1074/jbc.273. 33.20685
- Matsumoto, M., Togashi, H., Mori, K., Ueno, K., Ohashi, S., Kojima, T., & Yoshioka, M. (2001). Evidence for involvement of central 5-HT4 receptors in cholinergic function associated with cognitive processes: Behavioral, electrophysiological. And Neurochemical Studies. Journal of Pharmacology and Experimental Therapeutics, 296(3), 676-682.
- Matyash, V., & Kettenmann, H. (2010). Heterogeneity in astrocyte morphology and physiology. *Brain Research Reviews*, 63(1–2), 2–10. https://doi.org/10.1016/j.brainresrev.2009.12.001
- Mederos, S., González-Arias, C., & Perea, G. (2018). Astrocyte-neuron networks: A multilane highway of signaling for homeostatic brain function. Frontiers in Synaptic Neuroscience, 10, 45. https://doi.org/10.3389/fnsyn.2018.00045
- Minge, D., Senkov, O., Kaushik, R., Herde, M. K., Tikhobrazova, O., Wulff, A. B., ... Henneberger, C. (2017). Heparan sulfates support pyramidal cell excitability, synaptic plasticity, and context discrimination. *Cerebral Cortex* (New York, N.Y.: 1991), 27(2), 903–918. https://doi. org/10.1093/cercor/bhx003
- Mishra, A. (2017). Binaural blood flow control by astrocytes: Listening to synapses and the vasculature. *The Journal of Physiology*, *595*(6), 1885–1902. https://doi.org/10.1113/JP270979
- Miyazaki, I., & Asanuma, M. (2016). Serotonin 1A receptors on astrocytes as a potential target for the treatment of Parkinson's disease. *Current Medicinal Chemistry*, 23(7), 686–700. https://doi.org/10.2174/0929867323666160122115057
- Mlinar, B., Mascalchi, S., Mannaioni, G., Morini, R., & Corradetti, R. (2006). 5-HT4 receptor activation induces long-lasting EPSP-spike potentiation in CA1 pyramidal neurons. *European Journal of Neuroscience*, 24 (3), 719–731. https://doi.org/10.1111/j.1460-9568.2006.04949.x
- Muller, C. P., & Jacobs, B. (2009). Handbook of the behavioral neurobiology of serotonin. Cambridge, MA, USA: Academic Press. https://www. elsevier.com/books/handbook-of-the-behavioral-neurobiology-ofserotonin/muller/978-0-12-374634-4.
- Nusser, N., Gosmanova, E., Makarova, N., Fujiwara, Y., Yang, L., Guo, F., ... Tigyi, G. (2006). Serine phosphorylation differentially affects RhoA binding to effectors: Implications to NGF-induced neurite outgrowth. Cellular Signalling, 18(5), 704–714. https://doi.org/10.1016/j.cellsig. 2005.06.010
- Oberheim, N. A., Goldman, S. A., & Nedergaard, M. (2012). Heterogeneity of Astrocytic form and function. *Methods in Molecular Biology* (*Clifton, N.J.*), 814, 23–45. https://doi.org/10.1007/978-1-61779-452-0_3
- Oertner, T. G., Sabatini, B. L., Nimchinsky, E. A., & Svoboda, K. (2002). Facilitation at single synapses probed with optical quantal analysis. *Nature Neuroscience*, 5(7), 657–664. https://doi.org/10.1038/nn867
- Okamoto, K.-I., Nagai, T., Miyawaki, A., & Hayashi, Y. (2004). Rapid and persistent modulation of Actin dynamics regulates postsynaptic reorganization underlying bidirectional plasticity. *Nature Neuroscience*, 7 (10), 1104–1112. https://doi.org/10.1038/nn1311
- Parga, J., Rodriguez-Pallares, J., Muñoz, A., Guerra, M. J., & Labandeira-Garcia, J. L. (2007). Serotonin decreases generation of dopaminergic neurons from mesencephalic precursors via serotonin type 7 and type 4 receptors. *Developmental Neurobiology*, 67(1), 10–22. https://doi.org/10.1002/dneu.20306

- Peng, L., Verkhratsky, A., Gu, L., & Li, B. (2015). Targeting astrocytes in major depression. Expert Review of Neurotherapeutics, 15(11), 1299–1306. https://doi.org/10.1586/14737175.2015.1095094
- Ponimaskin, E. G., Profirovic, J., Vaiskunaite, R., Richter, D. W., & Voyno-Yasenetskaya, T. A. (2002). 5-Hydroxytryptamine 4(a) receptor is coupled to the G subunit of heterotrimeric G13 protein. *Journal of Biological Chemistry*, 277(23), 20812–20819. https://doi.org/10.1074/jbc.M112216200
- Rose, C. R., Felix, L., Zeug, A., Dietrich, D., Reiner, A., & Henneberger, C. (2018). Astroglial glutamate signaling and uptake in the hippocampus. Frontiers in Molecular Neuroscience, 10, 451. https://doi.org/10.3389/fnmol.2017.00451
- Rusakov, D. A., Bard, L., Stewart, M. G., & Henneberger, C. (2014). Diversity of astroglial functions alludes to subcellular specialisation. *Trends in Neurosciences*, 37(4), 228–242. https://doi.org/10.1016/j.tins.2014. 02 008
- Schill, Y., Bijata, M., Kopach, O., Cherkas, V., Abdel-Galil, D., Böhm, K., ... Ponimaskin, E. (2020). Serotonin 5-HT 4 receptor boosts functional maturation of dendritic spines via RhoA-dependent control of F-Actin. Communications Biology, 3(1), 1–16. https://doi.org/10.1038/s42003-020-0791-x
- Sheikhbahaei, S., Turovsky, E. A., Hosford, P. S., Hadjihambi, A., Theparambil, S. M., Liu, B., ... Gourine, A. V. (2018). Astrocytes modulate brainstem respiratory rhythm-generating circuits and determine exercise capacity. *Nature Communications*, 9, 370. https://doi.org/10.1038/s41467-017-02723-6
- Sibille, J., Pannasch, U., & Rouach, N. (2014). Astroglial potassium clearance contributes to short-term plasticity of synaptically evoked currents at the tripartite synapse. *The Journal of Physiology*, *592*(1), 87–102. https://doi.org/10.1113/jphysiol.2013.261735
- Stobart, J. L., & Anderson, C. M. (2013). Multifunctional role of astrocytes as gatekeepers of neuronal energy supply. *Frontiers in Cellular Neuroscience*, 7, 38. https://doi.org/10.3389/fncel.2013.00038
- Sugiyama, K., Tago, K., Matsushita, S., Nishikawa, M., Sato, K., Muto, Y., ... Ueda, H. (2017). Heterotrimeric G protein Gαs subunit attenuates PLEKHG2, a rho family-specific guanine nucleotide exchange factor, by direct interaction. *Cellular Signalling*, 32, 115–123. https://doi.org/ 10.1016/j.cellsig.2017.01.022
- Takemoto, K., Ishihara, S., Mizutani, T., Kawabata, K., & Haga, H. (2015). Compressive stress induces Dephosphorylation of the myosin regulatory light chain via RhoA phosphorylation by the adenylyl Cyclase/protein kinase a signaling pathway. *PLoS One*, 10(3), e0117937. https://doi.org/10.1371/journal.pone.0117937
- Teixeira, C. M., Rosen, Z. B., Suri, D., Sun, Q., Hersh, M., Sargin, D., ... Ansorge, M. S. (2018). Hippocampal 5-HT input regulates memory formation and Schaffer collateral excitation. *Neuron*, *98*(5), 992–1004.e4. https://doi.org/10.1016/j.neuron.2018.04.030

- Tkachenko, E., Sabouri-Ghomi, M., Pertz, O., Kim, C., Gutierrez, E., Machacek, M., ... Ginsberg, M. H. (2011). Protein kinase a governs a RhoA-RhoGDI protrusion-retraction pacemaker in migrating cells. *Nature Cell Biology*, 13, 660–667.
- Ullian, E. M., Sapperstein, S. K., Christopherson, K. S., & Barres, B. A. (2001). Control of synapse number by glia. *Science (New York, N.Y.)*, 291(5504), 657–661. https://doi.org/10.1126/science.291. 5504.657
- Wallraff, A., Odermatt, B., Willecke, K., & Steinhäuser, C. (2004). Distinct types of astroglial cells in the hippocampus differ in gap junction coupling. *Glia*, 48(1), 36–43. https://doi.org/10.1002/glia.20040
- Wu, Y. E., Pan, L., Zuo, Y., Li, X., & Hong, W. (2017). Detecting activated cell populations using single-cell RNA-Seq. *Neuron*, *96*(2), 313–329.e6. https://doi.org/10.1016/j.neuron.2017.09.026
- Wu, Y.-W., Tang, X., Arizono, M., Bannai, H., Shih, P.-Y., Dembitskaya, Y., ... Semyanov, A. (2014). Spatiotemporal calcium dynamics in single astrocytes and its modulation by neuronal activity. *Cell Calcium*, 55(2), 119–129. https://doi.org/10.1016/j.ceca.2013.12.006
- Yoshizaki, H., Ohba, Y., Kurokawa, K., Itoh, R. E., Nakamura, T., Mochizuki, N., ... Matsuda, M. (2003). Activity of rho-family GTPases during cell division as visualized with FRET-based probes. *The Journal* of Cell Biology, 162(2), 223–232. https://doi.org/10.1083/jcb. 200212049
- Zeug, A., Müller, F. E., Anders, S., Herde, M. K., Minge, D., Ponimaskin, E., & Henneberger, C. (2018). Control of astrocyte morphology by rho GTPases. *Brain Research Bulletin*, 136, 44–53. https://doi.org/10.1016/j.brainresbull.2017.05.003
- Zhang, Y., & Barres, B. A. (2010). Astrocyte heterogeneity: An underappreciated topic in neurobiology. *Current Opinion in Neurobiology*, 20(5), 588–594. https://doi.org/10.1016/j.conb.2010.06.005
- Zhou, B., Zuo, Y., & Jiang, R. (2019). Astrocyte morphology: Diversity, plasticity, and role in neurological diseases. *CNS Neuroscience & Therapeutics*, 25(6), 665–673. https://doi.org/10.1111/cns.13123

SUPPORTING INFORMATION

Additional supporting information may be found online in the Supporting Information section at the end of this article.

How to cite this article: Müller FE, Schade SK, Cherkas V, et al. Serotonin receptor 4 regulates hippocampal astrocyte morphology and function. *Glia*. 2021;69:872–889. https://doi.org/10.1002/glia.23933